Opto-thermo-mechanical phenomena in satellite free-space optical communications: survey and challenges

Badas Aldecocea, M.; Piron, P.; Bouwmeester, J.; Loicq, J.J.D.; Kuiper, J.M.; Gill, E.K.A.

Important note
To cite this publication, please use the final published version (if applicable).
Please check the document version above.

Opto-thermo-mechanical phenomena in satellite free-space optical communications: survey and challenges

Mario Badás [iD],* Pierre Piron [iD], Jasper Bouwmeester, Jérôme Loicq [iD], Hans Kuiper, and Eberhard Gill

Delft University of Technology, Space Engineering Department, Faculty of Aerospace, Delft, The Netherlands

ABSTRACT. Growing interest in free-space optical communication, due to the high bandwidth and security provided by these links, has generated the necessity of designing high-performance satellite terminals. In order to develop these terminals, the opto-thermo-mechanical phenomena that appear in the space environment and their effect on optical communication links have to be understood in detail. A review of the opto-thermo-mechanical phenomena occurring in spaceborne terminals is presented, describing the relevance of each of them. The methods found to compute the impact on the communication performance due to opto-thermo-mechanical phenomena are collected by building the bridge between the optical and communication performance parameters. Finally, techniques available to mitigate the detrimental effects of these phenomena are classified, and the relevant research challenges are identified.

1 Introduction

Due to an increasing demand for higher data rates and more secure communications, free-space optical communication (FSOC) has already shown to be a technology that could be a crucial part of future communication networks.[1] The higher bandwidth, directivity, and security, as well as lower power and mass requirements, make FSOC an interesting alternative to radiofrequency communication. The applications of this technology range from solving the last mile problem[2] to deep-space optical communications (DSOC).[3,4]

Satellite FSOC terminals are paramount for the further development of several applications, such as deep-space communications and Earth observation. These terminals have to be resilient to the severe space environment. Radiation, thermal, and mechanical loads in space will affect the operational performance of the components of the terminal. Furthermore, these terminals must be designed considering the limitations of spacecraft volume and mass. Hence, a profound understanding of the coupled opto-thermo-mechanical phenomena and their impact on the communication performance of the system is needed to identify requirements and optimize the design. This paper aims to explain the relevant opto-thermo-mechanical phenomena occurring in satellite terminals, identifying which of these phenomena are more important by providing a framework to evaluate the impact of these phenomena in FSOC. Furthermore, the

---

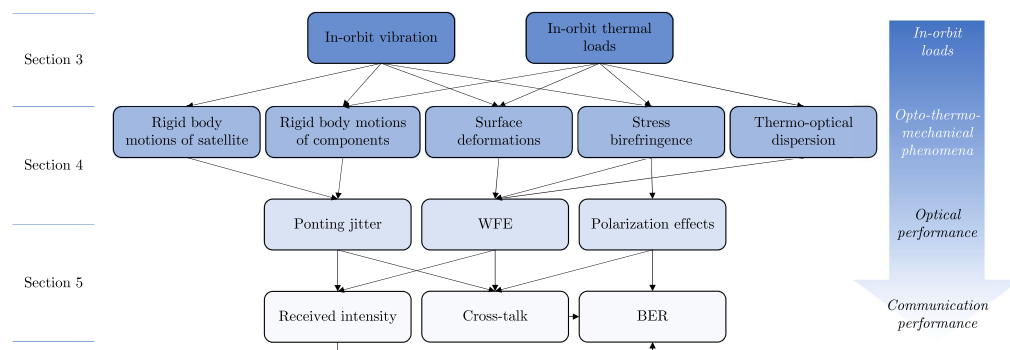*Address all correspondence to Mario Badás, m.badasaldecocea@tudelft.nl

Fig. 1 Structure of this paper emphasizing the main topics covered and the sections in which these are presented. The arrows represent the link between the different phenomena and parameters, relating the different causes to their respective effects (WFE, wavefront error and BER, bit error rate).

mitigation techniques to counteract these effects are classified and future research directions for the field are proposed.

In Sec. 2, a general satellite FSOC terminal is presented, describing its components and their function in the system. In Sec. 3, the mechanical and thermal loads to which satellite terminals are subjected in different orbits and scenarios are presented. The opto-thermo-mechanical phenomena occurring at the component level of the terminal are presented in Sec. 4, along with the effect that these have on the optical performance of the system. Furthermore, the modeling workflow to simulate these coupled multiphysics problems is presented, i.e., structural, thermal, and optical performance (STOP) analysis. Section 5 builds a bridge to translate the optical effects to communication performance parameters, to evaluate the impact on the communication due to the phenomena previously explained. This section will focus on the impact of opto-thermo-mechanical phenomena on intersatellite links, although the explanation could be generalized to other scenarios (i.e., satellite-to-ground) by considering also atmospheric effects. The mitigation techniques to decrease the detrimental impact of opto-thermo-mechanical phenomena in FSOC are presented in Sec. 6. Finally, future research topics in this area are proposed in Sec. 7. In Fig. 1, the structure of this paper is shown, and the relation between the phenomena, effects, and impact can be tracked.

2 System Overview

A satellite FSOC terminal will send or receive information modulated in a laser beam that travels through free space without the need of optical fibers to guide the light. To achieve this objective, a satellite FSOC terminal is formed by several optical components that steer and shape the beams going through it. Figure 2 shows a possible architecture in which the components that are relevant to the purpose of this paper are shown. The optical terminal will be in most cases capable of operating both as a receiver and transmitter (i.e., transceiver) as shown in this figure. The architecture presented has the objective of including the components to which opto-thermo-mechanical phenomena can be relevant and does not pretend to be an optimum architecture of an FSOC transceiver.

When transmitting a signal, the output data are modulated into the beam coming from the laser source. This transmitted beam is collimated and the point ahead angle compensates for the relative velocity with respect to the other terminal. By sending the laser beam to the location where the receiving satellite will be after the time it takes for light to travel from the transmitter to the receiver, the point ahead angle corrects for the relative velocities between the terminals. This angle is applied to the beam with the point ahead mirror in the architecture shown. Finally, the beam is transmitted through the telescope after being steered by the pointing and tracking mechanisms [i.e., fast steering mirror (FSM) and coarse pointing assembly (CPA)]. These mechanisms are controlled by the spot location of the light received in the CCD array and the quad cell, coming from the other terminal's beacon. When receiving the signal, a beacon is emitted from the receiver to enable tracking from the other transmitter. The received light is coupled into
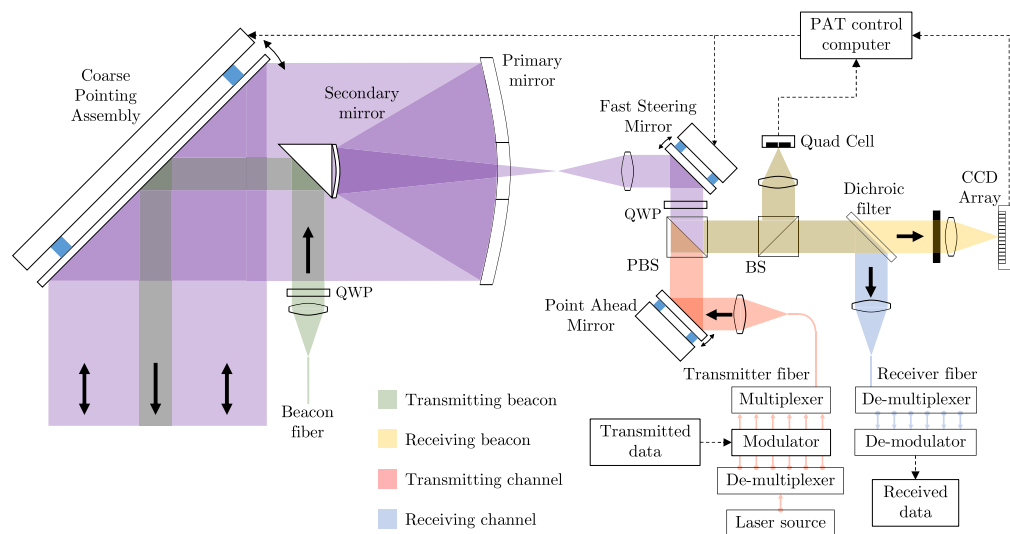
Fig. 2 General system diagram architecture for satellite FSOC transceiver terminal. The lenses shown are a simplified representation of lens assemblies. Colors not stated in the legend are combinations of others (BS, beam splitter; CCD, charge-coupled detector; PAT, pointing, acquisition and tracking; PBS, polarization beam splitter; QWP, quater waveplate).

a fiber and the data are extracted through demultiplexing and demodulation of it. Other architectures will include large free-space detectors instead of a fiber coupler.

There are different criteria that have to be considered when choosing a laser source for a satellite communication terminal, from the modulation and multiplexing techniques used to compatibility with optical fiber amplifiers.[5] Compatibility with optical fiber technologies in the design of FSOC terminals will enable the use of current fiber-optic technologies to improve the performance of the system. Such is the case of fiber amplifiers to amplify both transmitting[6] and receiving[7,8] signals.

The presented architecture in Fig. 2 shows a polarization beam splitter (PBS) to differentiate the transmitting and receiving waves, representing one of the many applications of the use of the polarization property of light in FSOC. Therefore, this paper will also study the effects on the polarization state of light due to opto-thermo-mechanical phenomena. Polarization can also be used in optical communications for multiplexing[9] and modulating the signal (polarization shift keying).[10–14] Polarization of light is also especially relevant for a technology that is closely related to FSOC, i.e., quantum communication.[15] Furthermore, several technologies used in optical communications terminals, such as wavelength division multiplexing devices, use the polarization of light as a baseline for their operation.[16] Finally, the polarization state of the beam has to be maintained in order to efficiently detect the beam in coherent detection receivers.[17] Considering all this, it is paramount to consider the changes in the polarization state induced by opto-thermo-mechanical phenomena in the terminal. The polarization state of light can linear, elliptical, or circular. For circularly polarized light, each photon carries a spin angular momentum (SAM). The left- and right-handed circular polarization states correspond to an SAM of $+\hbar$ and $-\hbar$, respectively.

Another property of light that can be exploited for communication purposes is the orbital angular momentum (OAM). The OAM is the momentum carried by a beam that is dependent on the spatial distribution of the electromagnetic field (polarization being the other component of angular momentum of light).[18] Using a set of orthogonal OAM states, this property can be used in FSOC for both modulation[19] or demultiplexing[20] (see Fig. 3). This property of light can be combined with other modulation and demultiplexing techniques that exploit other properties of light, e.g., wavelength, phase, and polarization.[13] Figure 4 shows the different modulation techniques using the polarization and OAM properties of light. The reader can therefore verify the difference between these two angular momenta; whereas the helicoid exploiting SAM to modulate the encoded information represents the polarization status of the whole wavefront, the one using OAM represents the spatial distribution of the wavefront.
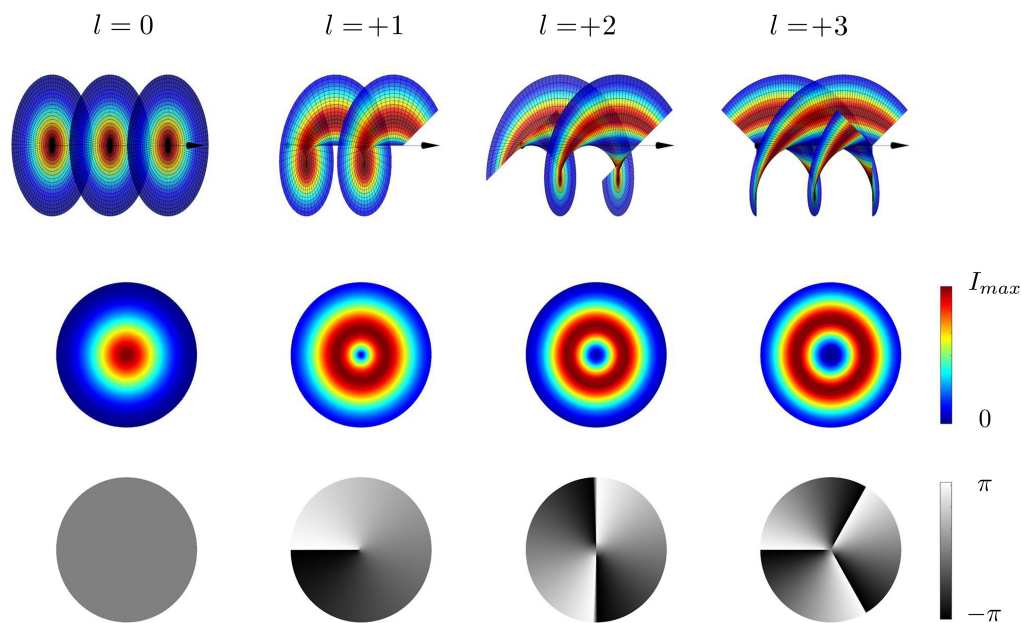
Fig. 3 OAM of Laguerre–Gaussian beams. The radial zeroth order of the modes is shown for different *l* azimuthal orders. The wavefront, the intensity profile, and the phase for each OAM mode given by the order *l* are shown in the first, second, and third rows, respectively. The negative values of the *l* order will yield a different handedness of the helical wavefront conserving the intensity profile.
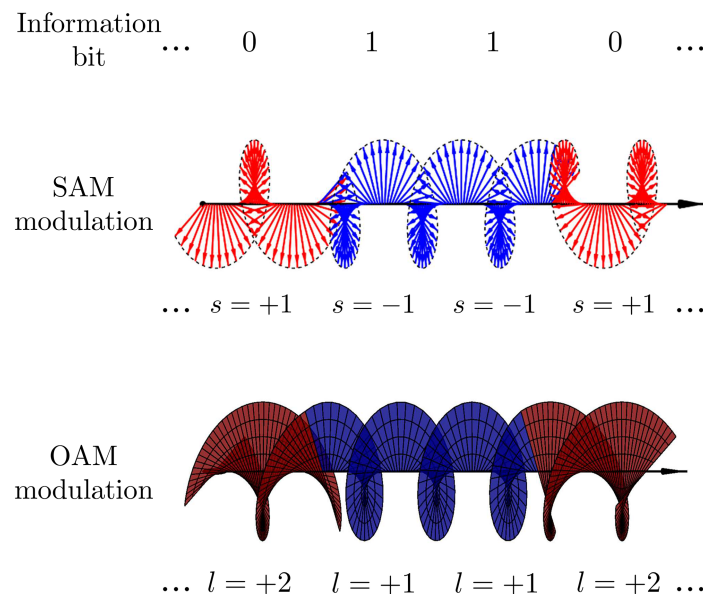
Fig. 4 Schematic diagram showing the use of SAM and OAM modulation, respectively. The SAM states $s = \pm 1$ and the OAM states $l = +1$, $+2$ are used as an example.

Furthermore, different wavelengths are used in the proposed architecture for the received beacon and channel to differentiate them with a dichroic filter. The selection of the wavelength to be used in a communication link is dependent on several factors, such as the atmospheric effects, availability of technology, and safety regulations. When the FSOC laser beam travels partially or totally through the atmosphere, the wavelength selection is mainly done by attending to the reduction of detrimental atmospheric effects (absorption, rain, fog, and turbulence). Several of these reasons support using the near-infrared spectra as the main range of interest for FSOC.[21] Wavelengths on the mid-wavelength and long-wavelength infrared have also been

Table 1 Properties of light used in FSOC and a brief description of how they are affected by opto-thermo-mechanical phenomena. Tx/Rx refers to the separation between transmitting and receiving light.

Property	Use in FSOC	Effect of opto-thermo-mechanical phenomena
Amplitude	Modulation	A minimum amplitude of the light field is required on the receiver side in order to detect the signal. The amplitude of the light field entering the receiver is affected by opto-thermo-mechanical phenomena (see Sec. 5)
Phase	Modulation, multiplexing	Apart from phase modulation, the spatial distribution of the field's phase can generate orthogonal beam modes that can be used for multiplexing. Unexpected changes in the phase due to opto-thermo-mechanical phenomena are detrimental for the system
Wavelength	Modulation, multiplexing, Tx/Rx	The wavelength of the light field is a key link parameter mainly dependent on the channel characteristics (atmosphere, vacuum, etc.) and available hardware. Deformations of optical components due to opto-thermo-mechanical phenomena can be more restrictive in shorter wavelengths (see Sec. 5.2)
Polarization	Modulation, multiplexing, Tx/Rx	The polarization state of light can be perturbed by opto-thermo-mechanical phenomena, yielding to crosstalk and BER (see Sec. 5.5)

proposed to lower the detrimental atmospheric effects in the link.[22–24] Furthermore, the role that the wavelength of the light plays in FSOC becomes paramount when using wavelength division multiplexing to increase the capacity of the channel.

In general, all properties of light (amplitude, phase, wavelength, and polarization) can be exploited with a different purpose in an FSOC satellite terminal (see Table 1). This will provide a large number of design possibilities to optimize the performance of the system. In order to assure the correct operation of the system, the effects of the environmental conditions encountered in space on the performance of the terminal must be thoroughly assessed.

3 Space Environment

Satellite FSOC terminals will have to survive the harsh space environment consisting of radiation, plasma, thermal, and mechanical loads. Furthermore, these terminals and their constituting components will have to operate correctly in this environment. In this section, only the mechanical and thermal environments encountered in space are treated. An overview of other space environmental conditions was presented by Lu et al.[25] These other environmental conditions will also affect the performance of the FSOC system and have to be considered during the design of the terminal. For example, radiation effects can be especially harmful to the optical components[26] and laser sources[27] required to build such a terminal.

The mechanical and thermal loads impinged on a satellite will affect the performance of the communication link through different opto-thermo-mechanical phenomena (Sec. 4). The sources and magnitudes of the mechanical and thermal loads on a satellite have to be studied in order to quantify their effects on FSOC.

3.1 Microvibrations

Due to the narrow beam divergence (usually smaller or equal to milliradians), FSOC systems require a high pointing accuracy (in the order of microradians) to minimize the average bit error rate (BER). The main source of pointing error in an FSOC satellite terminal is the vibration of the satellite due to different in-orbit sources. These in-orbit vibration sources can be classified into internal and external vibration sources.[28]

- *External vibration sources*. They are due to loads coming from outside the satellite, such as solar radiation pressure, micrometeorite/space debris impacts,[25] elastic forces of tension/bending, and gravitational dynamic effects (solar and lunar gravity, Earth oblateness effects, ellipticity of orbit, or Earth's central gravitational field).
- *Internal vibration sources*. They are due to loads originating inside the satellite, such as solar array mechanism, thruster operation, pointing, acquisition, and tracking (PAT) mechanisms, gyroscope noise, and attitude actuators based on angular momentum (e.g., reaction wheels).[29]

Other sources of vibrations that could be relevant for future FSOC satellites are the vibrations induced by a cryocooler. The cryocooler could be needed to operate superconducting nano-wire single-photon detectors in future FSOC satellites.[30] The microvibrations induced by this turbomachinery can contribute significantly as it was shown in the Hubble Space Telescope.[31]

To quantify the contribution of each vibration source to the overall satellite vibration, in-orbit measurements of the vibration have been done on FSOC satellites. Given the multiple sources of microvibrations and their statistical nature, experimental in-orbit measurements of these are especially relevant.[32] A review of the in-orbit microvibration detection methods is presented by Tang et al.[33] In Fig. 5, the in-orbit measurements of the power spectral density (PSD) of the angular microvibrations for the most relevant missions are shown. This figure shows similar trends for all the missions and specifications collected. In particular, it can be seen that the energy due to angular microvibrations is mainly concentrated at frequencies lower than 30 Hz for Micius and Olympus, 100 Hz for OICETS, and 102 Hz for ETS-VI.[34]

The in-orbit measurements done through a three-axis accelerometer package onboard the Olympus satellite[35] set the ground for the characterization of the vibration environment of an optical communication payload onboard a satellite. This experimental campaign quantified the relative weight of each of the internal vibration sources. The typical duration of internal sources that are relevant to the FSOC satellite terminals can be found in the literature.[38,39] This analysis shows that the longest lasting source of vibrations onboard the Olympus satellite is the antenna pointing mechanism (in the order of seconds).

More recent in-orbit measurements of microvibrations for the OICETS FSOC satellite were presented by Toyoshima et al.[36] The authors of this work reported that the worst-case angular microvibration are created during the tracking and slewing operations of the gimballed optical antenna. The angular microvibrations onboard the Micius quantum communication satellite and the suppression of these with the PAT mechanism are presented by Wang et al.[34]
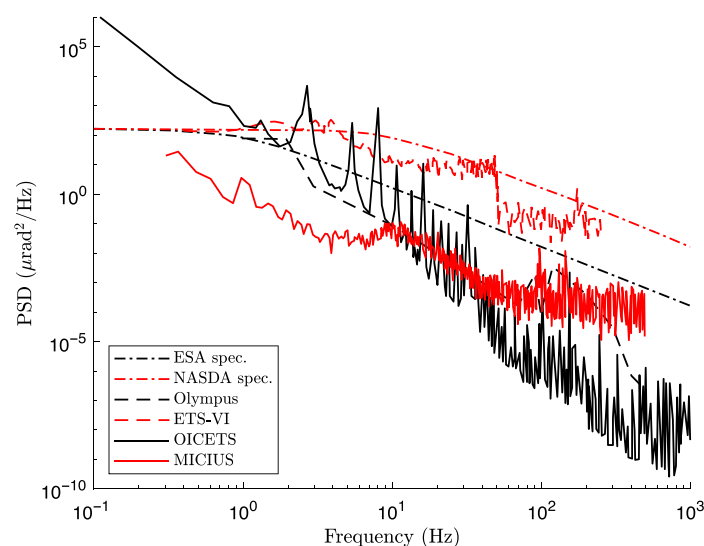

Fig. 5 In-orbit measurements of vibration PSD of the angular displacement for different space missions. ESA spec. and NASDA spec. refer to the specifications set by the respective space agencies, whereas the rest are in-orbit measurements of different satellites. Data extracted from Refs. 34–37.

The analysis of the in-orbit measurements of other internal vibration contributors, such as the control momentum gyroscope, the solar array mechanism, and the reaction wheel, was reported by Yu et al.[32] This work concludes that in the absence of an optical gimbal antenna mechanism, the main contributors to satellite vibrations are the control moment gyros and reaction wheels.

Another source of microvibrations in space that has been studied in depth is a coupled thermo-mechanical phenomenon known as the thermal snap. This phenomenon occurs when the solar arrays (which are usually the most flexible structure in the satellite) are subjected to rapid changes in temperature when entering or leaving an eclipse. This phenomena are mainly due to a varying temperature gradient across the thickness of the solar panels.[40] In-orbit measurements of the thermal snap, phenomena were presented by Oda et al.[41] As it is presented in Sec. 6, several techniques can be implemented to reduce some of the microvibrations sources presented in the previous paragraphs.

3.2 Thermal Loads

Due to the orbit around the Earth, a satellite will be subjected to large temperature gradients during an orbital period. Inside an FSOC terminal, there are optical elements that are sensitive to these temperature variations. As it will be explained in the next section, the thermal loads on the optical elements, such as lenses and mirrors, can deviate from their nominal performance yielding a detrimental effect on the FSOC link. Therefore, it is paramount to know the thermal loads to which the satellites in different orbits will be subjected.

Due to the high to ultra-high vacuum environment encountered in space, radiation is the dominant heat transfer mechanism of the satellite with the external environment. Figure 6 shows the external radiation heat loads that appear in the space thermal environment.

The solar radiation from the Sun will impinge the satellite with an ~ 1361 W/m^2 at one astronomical unit in a plane normal to the vector direction to the Sun.[42] For a satellite in orbit around the Earth, this value is not constant due to various factors, such as the solar forcing[43] or the ellipticity of the Earth's orbit around the Sun (that results in a change in the distance between these two). On the other hand, when the satellite enters the shadow of the Earth, this heat load disappears and the cooling down of the whole satellite occurs, until it is heated again at the exit of the shadow. Some of the sunlight is reflected on the Earth yielding to the short-wavelength albedo radiation, which will be dependent on the location and time of each of the Earth's locations. Measurements of the albedo coefficients necessary to accurately quantify this heat load can be found in the literature.[44] The Earth-emitted radiation creates long-wavelength radiation also known as Earth orbital long-wavelength radiation (OLR) that will also be part of the space thermal environment. The time and location-dependent measurements of this radiation can be found in Ref. 45. Finally, due to the background radiation of outer space at ~ 2.7 K, the satellite will irradiate heat toward it.

Another external source of heat in space is the charged-particle heating,[46] which is due to collisions of the charged particles trapped in the Van Allen belts with the spacecraft. This mode of heating is usually confined to the first hundredth of a centimeter from the material surface and is much weaker than the radiation heat sources stated above. These heat loads can have relevant
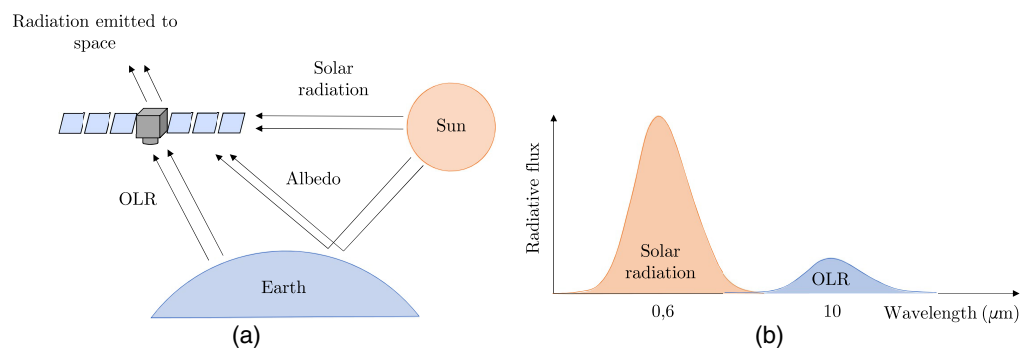

Fig. 6 (a) External thermal loads of a satellite in orbit around the Earth. (b) The qualitative spectrum of the direct solar radiation and the Earth OLR.

contributions in spaceborne cryogenic systems,[47] such as the future superconducting nanowire single-photon detectors for FSOC.[30,48] For example, a radiator designed for 70 K steady-state operation in a circular equatorial Earth orbit at 3200 km altitude will increase its temperature by 2.9 K.[46]

The phenomena explained above will altogether set a periodic transient temperature for a satellite in-orbit. Low Earth orbit (LEO) is where most of the satellites are placed nowadays. In LEO, defined as 160 to 2000 km altitude,[25] the satellite has an orbital period equal or <128 min. The thermal loads for a satellite in LEO will change in each orbit due to the changing thermal environmental parameters in time (i.e., albedo coefficient, direct solar irradiance, and OLR). The analysis done by González-Bárcena et al.[42] presents a methodology to obtain the worst-case thermal scenarios for a satellite in LEO taking into account the variation of these parameters in time. This analysis derives temperatures in the 150 to 210 K range, for a satellite in a Sun-synchronous orbit. Furthermore, an analysis for different solar beta angles (the beta angle is the angle between the orbital plane of the satellite and the geocentric position of the Sun) to select the worst-case thermal environment was developed by Hengeveld et al.[49] The guidelines and methodologies developed by NASA to obtain the worst-case thermal scenario in LEO can be found in the literature.[50,51] The approach followed by Yenchesky et al.[52] for the thermal analysis of an FSOC CubeSat is characterizing statistically the environmental thermal parameters and computing a Monte Carlo simulation.

The geosynchronous orbit (GEO) is defined as an orbit with an orbital period that matches Earth's rotation, the most famous of which is the GEO. The thermal environment for a satellite in GEO can be calculated with the same methodologies that are presented by González-Bárcena et al.[42] for LEO. Another approach followed by Zhang et al.[53] is to neglect both the albedo and OLR heat flows considering only the prevalent direct solar radiation at these altitudes.

There is also an increasing interest in using FSOC for the communication systems to transfer scientific data from deep-space probes back to Earth.[3,54] The thermal environment in such a scenario can be quite diverse due to the broad spectra of missions and trajectories found in deep space. The external radiation heat loads in deep-space probes will be due to the albedo and self-emitted radiation of other planets and asteroids (such are the cases of the LLCD,[55] MLCD,[56] and DSOC onboard Psyche mission[57]). In addition, the direct solar radiation will also change as a function of the distance to the Sun and therefore this value has to be accurately reevaluated in each of the scenarios. An overview of the specific characteristics of the thermal environment around other solar system objects is presented by Gilmore.[46]

On top of that, internal heat loads will also appear due to the operation of different systems onboard the satellite, such as Joule dissipation in circuits, the propulsion system,[58] the laser source,[59] or the cryocooler.[60] Optical amplifiers used onboard satellite to amplify the power of the beam coming from the source can also be an important source of heat.[61] Optical amplifiers, e.g., erbium-doped fiber amplifier (EDFA), with output optical powers on the order of watts dissipating tens of watts of heat, can be severely self-heated in satellite terminals.[62] The self-heating of these devices not only limits their performance[63] but also usually limits their duty cycle.[64] These sources of internal heat load can be enough to generate optical misalignment issues onboard the terminal.[65] Finally, the laser beam itself can be a significant thermal load in small components without enough thermal sinking. Such is the case of microelectromechanical FSMs.[66] For satellite FSOC terminals, the thermal lensing effect[67,68] is usually negligible due to the low powers (maximum 10 W average power) used in satellite transmitter lasers.[17]

4 Opto-Thermo-Mechanical Phenomena

The mechanical and thermal loads in an optical terminal in space will induce displacements, deformations, and changes in the index of refraction. These effects will in turn deviate the system from the nominal optical performance and therefore have to be well understood and analyzed during the design process of the FSOC space terminal. In this section, the relevant opto-thermo-mechanical phenomena are presented and their effects on the optical performance of the system are discussed. The classification of these phenomena has been done by attending to the physical description and modeling techniques that are used to quantify them (see Fig. 1).

The effects on the optical performance of the system are quantified by three different optical performance parameters that are relevant to FSOC: pointing jitter, wavefront error (WFE), and polarization state (see Fig. 1). The pointing jitter refers to the dynamic angular error between the communication line of sight and the optical axis of the terminal (transmitter or receiver). In this paper, the WFE is used to quantify the optical aberrations due to the opto-thermo-mechanical phenomena explained below. Other parameters, such as the Strehl ratio,[69] can also be used to evaluate the optical performance in FSOC. Finally, changes in the polarization state created by opto-thermo-mechanical phenomena will also be relevant to the performance of the system and will be quantified by means of the polarization extinction ratio (PER).

4.1 Satellite Rigid Body Angular Displacements

At the largest scale of the system, the vibrations of the satellite will induce rigid body angular displacements of the whole satellite. These rigid body displacements will in turn create a pointing jitter and therefore deteriorate the performance of the link.

The satellite's rigid body angular displacements will be mainly due to the in-orbit induced microvibrations. The highly stochastic nature of these microvibrations and their high dependency on the interfaces and the details of the satellite[70] make experimental measurements the most valuable to understand the dynamics of the satellite as a whole (such as the in-orbit results shown in Fig. 5). The angular deviation of the satellite with respect to the optical axis is statistically characterized by a probability density function (PDF) for the satellite's angular pointing error $\theta^2 = \theta_E^2 + \theta_A^2$, where θ_E and θ_A are the elevation and azimuth pointing errors, respectively. For a zero-centered normal PDF in both azimuth and elevation pointing error, the PDF of the angular pointing error is a Rayleigh distribution given by the following equation:[71]

$$p(\theta) = \frac{\theta}{\sigma^2} \exp\left(-\frac{\theta^2}{2\sigma^2}\right), \tag{1}$$

where σ^2 is the variance of the radial pointing error. For a normal PDF non-centered in zero in both elevation and azimuth angles, a positive angular static error (also referred to as foresight pointing error or static printing error in the literature) has to be included. In this case, the PDF containing pointing jitter and static error will be given by a Rician distribution:[72,73]

$$p(\theta, \phi) = \frac{\theta}{\sigma^2} \exp\left(-\frac{\theta^2 + \phi^2}{2\sigma^2}\right) \mathcal{J}_0\left(\frac{\theta\phi}{\sigma^2}\right), \tag{2}$$

where ϕ is the angular static error and $\mathcal{J}_0$ is the zeroth order Bessel function. For the remaining analysis in this paper, the boresight error is taken into account through the PDF of the pointing jitter. Hence, from the experimentally obtained time series of microvibrations in-orbit, the variance σ^2 can be derived. The PDF constructed with this value will characterize the performance of the communication as explained in Sec. 5.

4.2 Rigid Body Motions of Optical Components

The satellite microvibrations and the thermal loads can also induce rigid body motions of the optical components inside the satellite.[74] These rigid body motions will, in turn, induce pointing jitter, defocus, and other high-order optical aberrations [see Fig. 7(a)].

In order to model the effects on the optical performance of the system due to rigid body displacements induced by in-orbit random vibrations in the satellite, finite-element analysis (FEA) can be computed to obtain the natural frequencies and mode shapes of the optical system. The pointing sensitivity coefficients (also referred as line of sight sensitivity coefficients in the literature) can be calculated by obtaining the pointing error due to unitary displacements on each of the degrees of freedom that are being analyzed. Then the frequency response function (FRF) is obtained using modal analysis, and the PSD response is obtained through the FRF and the input force PSD functions. Finally, the pointing jitter can be obtained via the pointing sensitivity coefficients.[75,76] An analysis of the pointing jitter for the FSOC terminal of the Mars Laser Communications Demonstration Project is presented by Doyle.[77]
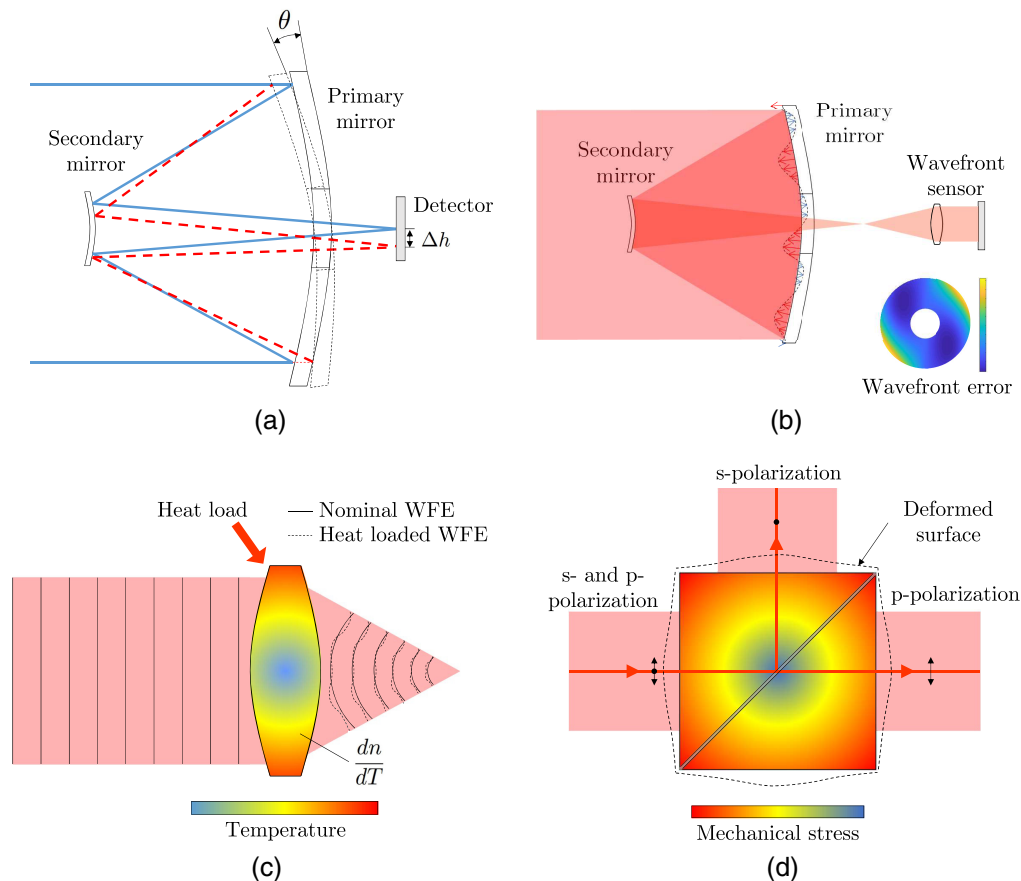
Fig. 7 Opto-thermo-mechanical phenomena: (a) rigid body motions of optical components inducing pointing jitter; (b) surface deformations of optical components inducing WFE; (c) thermal dispersion on refractive elements; and (d) stress birefringence in a PBS.

4.3 Surface Deformations of Optical Components

In case the vibrations of the satellite are strong in magnitude, significant elastic deformations will be induced in the optical surfaces. Thermal loads will also create thermo-elastic deformations of the surfaces of the optical components. These, in turn, will create optical aberrations [see Fig. 7(b)] that will also affect the performance of the link. Surface deformations will occur together with changes in volume on the optical components that affect the optical path length (OPL). The thermo-elastic phenomena are partially governed by the properties of the materials in the optical assembly of the system. The relevant thermo-elastic properties for the materials used in the infrared are discussed in detail by Klocek.[78]

Surface deformations induced by thermal static or transient loads are usually computed through FEA and/or finite difference analysis.[79] The heat transfer problem can be computed through any of the methods while the thermo-elastic problem is usually solved by FEA.[53,80–82]

To compute surface deformations induced by in-orbit vibration loads, the surface deformations are computed with FEA and statistical energy analysis (SEA). The first is used to obtain the response to low-excitation frequencies, which enable a more deterministic analysis of the system. SEA[83] is used to compute the behavior of the system for high-excitation frequencies because the deterministic methods become too sensitive to structural details for these frequency bands[70] (see Fig. 8). Other approaches consist of using stochastic FEA or hybrid FEA–SEA models.[84]

4.4 Thermal Dispersion on Refractive Optical Components

Refractive optical materials used in FSOC components exhibit a temperature-dependent index of refraction. The dependence on the index of refraction due to the variation of temperature can be expressed as[85]
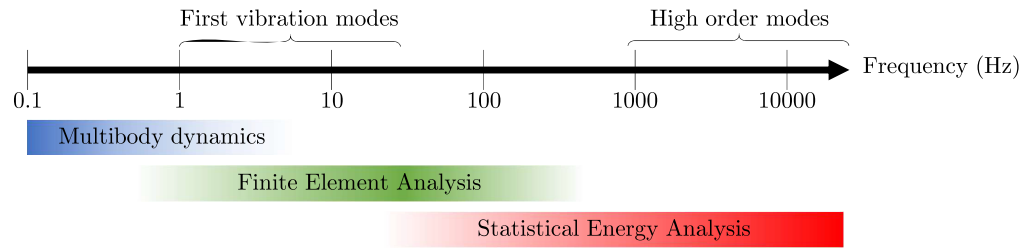
Fig. 8 Modeling techniques for vibration transmission for different frequency bands (adapted with permission from Ref. 70).

$$\frac{dn}{dT} = \left(\frac{\partial n}{\partial T}\right)_\rho + \left(\frac{\partial n}{\partial \rho}\right)_T \left(\frac{\partial \rho}{\partial T}\right). \tag{3}$$

The first term is the change in the index of refraction solely due to the change in temperature, whereas the second term represents the change in the index of refraction due to the temperature-induced change in the densities of the material. A detailed theoretical expression of each of the terms presented above can be obtained through the theory of thermo-optic dispersion for solids presented in Refs. 86 and 87. It is important to remark that although the coefficient of thermal expansion is also represented in Eq. (3) through the factor $\partial \rho / \partial T$, the optical path difference created in a ray due to the thermal expansion of the material has to be added to that created by the change in the index of refraction. Hence, the OPL and therefore the WFE for a thermally loaded material must be computed as

$$\text{OPL} = \int_0^{L'} n(s, T) \mathrm{d}s, \tag{4}$$

where s is the path followed by the ray, $n(s)$ will be obtained through dn/dT, and L' is the thermally expanded length of the path that the ray travels. The thermally induced optical path difference is obtained directly by combining the two factors explained above: the change in the index of refraction and the thermal expansion of the material.[88,89] The thermo-optic coefficients for the typical materials used in infrared refractive optical components are presented by Klocek.[78] Rogers et al.[90] analyzed the importance of the accuracy in the value of dn/dT for large operational temperature range scenarios (as could be the one for satellite FSOC terminals). The importance of making custom measurements of this parameter for wide operational temperature range applications is emphasized in the study.

The thermal load will induce a gradient index profile in the optical component that results in a non-nominal OPL for each ray,[91] and therefore, a WFE as illustrated in Fig. 7(c). Two ways of computing the thermal dispersion in refractive components with ray tracing algorithms are discussed by Michels et al.[91]

4.5 Stress Birefringence of the Optical Refractive Components

Finally, stress states due to the external loads on the refractive optical components will create a stress status that will induce birefringence. Optical birefringence is an anisotropic phenomenon, in which the index of refraction of the material depends on the polarization and the propagation direction of light. Some materials are birefringent in nature, whereas others will become birefringent when subjected to a stress field. In the latter, the stress field will vary the dielectric impermeability tensor β_{ij}, therefore, varying the index of refraction of the material in an anisotropic manner.[16] Mathematically, this phenomenon is usually represented via the stress-optical coefficient tensor q_{ijkl}:

$$\Delta \beta_{ij} = q_{\text{ijkl}} \sigma_{kl}, \tag{5}$$

where σ_{kl} are the components of the stress state tensor in each point of the domain and the subindices represent the spatial coordinates. For isotropic materials, the variation in the dielectric impermeability will create a difference between the two principal optical indices in the electromagnetic waves perpendicular to the ray direction. Hence, the principal optical axes will coincide with the principal stress axes and retardation between the orthogonally polarized waves will be
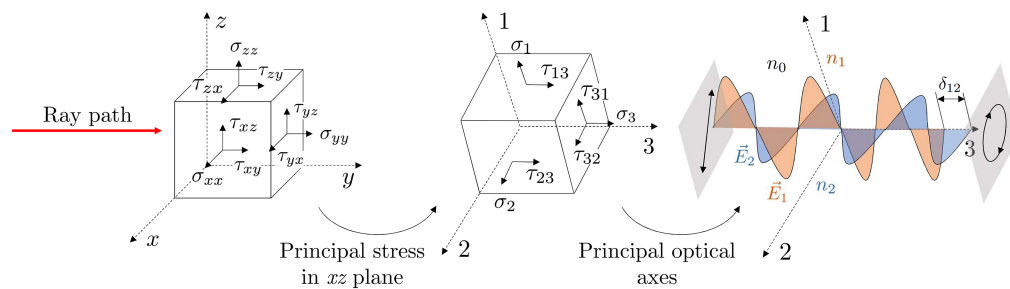
Fig. 9 WFE induced by stress birefringence in optical components. The linear polarization of the incoming ray is changed to an elliptically polarized one. σ_{ij} and τ_{ij} are the normal and shear stress components of the element. δ_{12} is the retardation induced by the stress state between the light polarized parallel to the optical axes 1 and 2. Being 1 and 2 the principal stress axes perpendicular to the ray path.

produced as depicted in Fig. 9. This retardation is equivalent to a change in the polarization state of the beam. Furthermore, the phase retardation in each of the optical principal axis components of the electromagnetic wave will induce a WFE in the light that can be approximated as the average of the OPL differences of each of these components.[82] Moreover, the beam will be split into two beams due to the birefringence, but this effect is so small in FSOC that can be usually neglected.[92]

For an isotropic material, subjected to a hydrostatic stress state, Eq. (5) will yield an isotropic index variation. Therefore, in the latter, no change in the polarization state will be induced by the hydrostatically stressed element. Hence only stress dispersion of the index of refraction will be occurring in this element, i.e., an isotropic variation of n.

The stress birefringence phenomena can be modeled with Jones calculus[93] by transforming the Jones vector through rotation and retardation matrices as presented by Yiu and Meyer.[92] Jones calculus represents the polarized light as a vector and the optical components are represented as matrix operations changing these vectors. To compute the effects of stress birefringence, the Jones matrice of the stressed element has to be computed. In order to do so, the stress state tensor in the domain points encountered by the ray path has to be obtained in an FEA structural mechanics software.[92,94,95] When the optical modeling of the system under study is done through wave optics instead of ray tracing, Eq. (5) is used to compute the variation on the index of refraction in every direction in each element of the domain, and the wave equations are solved assigning the calculated values to each element in the domain.[96] The effect of stress-induced birefringence in a cube PBS used in an optical circulator (widely used in FSOC systems) is analyzed by Doyle and Bell,[97] where the effect of the temperature and stress in the WFE and the polarization state are analyzed through a combination of FEA and ray-tracing software.

In an FSOC terminal onboard satellite, the opto-thermo-mechanical phenomena explained above act altogether creating a strongly coupled opto-thermo-mechanical problem. Therefore, to simulate the optical performance of the system, all the phenomena above have to be included simultaneously in the model. The approach for modeling opto-thermo-mechanical phenomena combining mechanical, thermal, and optical modeling techniques is presented in Fig. 10. These multiphysics modeling techniques that analyze the coupled opto-thermo-mechanical phenomena are generally referred to as STOP analysis in the literature.[82,98–100] As shown in Fig. 10, there are cases in which the opto-thermo-mechanical analysis has to be done in an iterative process, such as when the laser beam itself is the source of heat.[66] This is usually not the case for FSOC, and the vast majority of opto-thermo-mechanical phenomena can be characterized by following the diagram in Fig. 10 non-iteratively from top to bottom. The thermal and mechanical effects in the optical performance can be analyzed with several analytical and/or numerical methods depending on the complexity of the problem that is being modeled. Analytical methods can be used when the boundary conditions and the geometry of the system are simple. The increasing complexity of any of them increases the necessity of numerical methods to model the problem. A summary of the different commercial software available to model opto-thermo-mechanical problems is presented by Heijmans et al.[101] An example of a complete STOP analysis done by combining the methods presented in this section is given by Driscoll et al.[102] for the beam expander telescope
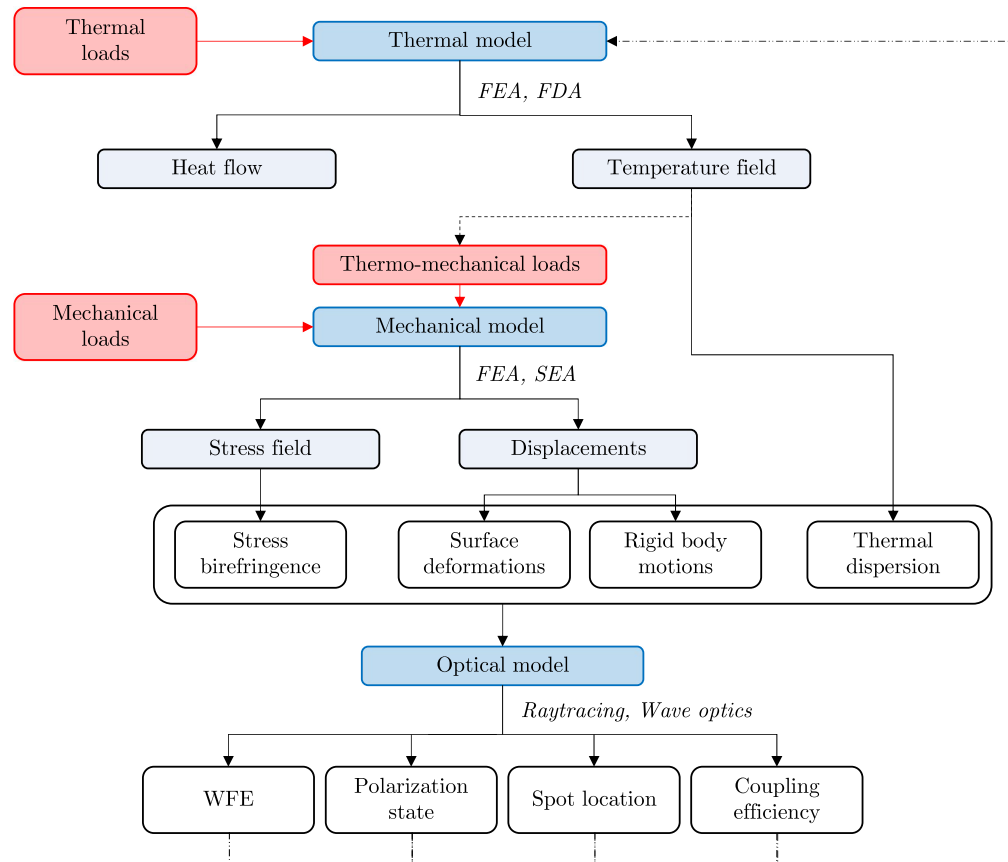
Fig. 10 Road-map for modelling opto-thermo-mechanical phenomena, STOP analysis. The loads (boundary conditions necessary to solve the problem) are shown in red boxes. The models and their results are shown in blue and light blue boxes, respectively. Finally, the parameters to characterize opto-thermo-mechanical are shown in white boxes. The dash-point line shows the iterative process for scenarios in which the optical performance determines the thermal loads.

onboard the NASA Psyche DSOC mission. The STOP analysis performed enables the calculation of the permitted WFE to maintain the beam divergence required below 14.5 μrad over a temperature range of 80°C. Furthermore, some of the key challenges, such as maintaining the alignment between the primary and secondary off-axis mirror, are discussed.

The optical performance of the system has been characterized via pointing jitter, WFE, and polarization state in this section. In the next section, how these optical parameters affect the communication performance on an FSOC link is explained.

5 Impact of Opto-Thermo-Mechanical Phenomena on FSOC

The pointing jitter, aberrations due to WFE, and polarization state changes induced by the opto-thermo-mechanical phenomena on the optical terminal onboard the satellite will impact the performance of the FSOC link. This section presents the methods to quantify the impact on the communication link due to these phenomena. A classification has been created according to where the phenomena occur (transmitter or receiver) and the type of optical effect created by these (jitter, WFE, or polarization change). In the following sections, the impact on communication of each of these effects acting separately is explained. It is worth mentioning that while some FSOC terminals act as transceivers, the classification presented below aims to separate the opto-thermo-mechanical effects in any terminal acting either as a transmitter or a receiver. In the remainder of this section, the use of transmitter and receiver terminals refers to terminals (that also include transceivers) operating as such.

To evaluate the impact of the phenomena above presented in the communication performance, the effect of these phenomena in the transmission equation is evaluated first.

The transmission equation is used in FSOC to evaluate the value of the signal intensity at the receiver's detector. The Friis transmission equation can be written as[71]

$$P_R = P_T G_T \mu_T L_S L_{\text{PJT}} L_A G_R \mu_R \mu_C, \qquad (6)$$

where P_R is the instantaneous received power, P_T is the average transmit power, G_T is the transmit antenna gain, μ_T is the transmitter feeder loss, L_S is the space loss, L_A is the term grouping all atmospheric effects, L_{PJT} is the transmitter pointing jitter loss, G_R is the receiver antenna gain, μ_R is the receiver transmission loss, and μ_C is the fiber coupling loss. (Atmospheric effects are not considered in this paper. Opto-thermo-mechanical phenomena onboard satellites will not impact the value of L_A.)

Furthermore, the different noise sources appearing in the communication link can be computed to obtain the total noise.[17] Combining the transmission equation and the noise, the signal-to-noise ratio (SNR) of the communication link can be obtained. The probability that a transmitted information bit is read incorrectly at the receiver is called the BER. The BER is evaluated through the SNR of the communication link according to the modulation technique used.

The impact on the communication performance of the opto-thermo-mechanical phenomena stated above is evaluated by assessing how these phenomena alter the values of the received intensity, the cross-talk between multiplexed signals, and finally the BER (see Fig. 1). In what follows, satellite-to-satellite links are mainly discussed to quantify the impact of opto-thermo-mechanical phenomena. Satellite-to-satellite scenarios are discussed because of the absence of atmospheric effects in the link, hence isolating the impact of opto-thermo-mechanical phenomena solely. However, the phenomena discussed in this section can be translated to other scenarios (e.g., satellite-to-ground) by including the relevant atmospheric effects.

5.1 Transmitter Pointing Jitter

In order to assess the impact of the pointing jitter and the aberrations in the communication link, a distinction must be made according to where these phenomena occur, i.e., in the transmitter or in the receiver. For the sake of explanation, an intersatellite communication scenario is considered. The pointing jitter in the transmitter (Fig. 11), created primarily due to the rigid body motions of the satellite and the optical components in the terminal due to microvibrations, will degrade the communication by diminishing the signal intensity received in the receiver's aperture [see Fig. 12(a)]. This is usually quantified in the link budget by introducing a pointing jitter loss L_{PJ} in the transmission equation [Eq. (6)]. In general, the contribution of the microvibrations to the pointing jitter will be added to many other pointing errors (see figure 2.2 in Ref. 17). The instantaneous loss due to the transmitter pointing jitter can be expressed for a Gaussian beam at the aperture of the transmitting telescope as[103]

$$L_{\text{PJT}} = \exp(-G_T \theta_T^2), \qquad (7)$$

where G_T is the antenna gain and θ_T is the angle radial pointing error. For a Gaussian, non-aberrated beam, the wavefront at sufficiently large distances (when the distance between the terminals is much bigger than the Rayleigh range) will be a spherical surface centered on the transmitter terminal. Hence, the electromagnetic field entering the aperture of the receiver can be
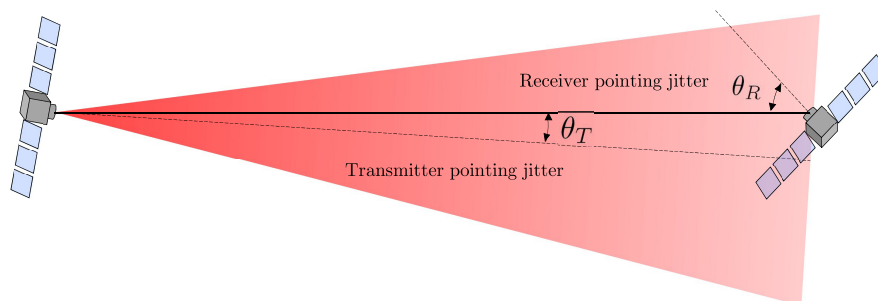

Fig. 11 Definition of the transmitter and receiver pointing jitter. The continuous line represents the direct line of sight between the transmitter and the receiver, connecting the central point of both apertures.
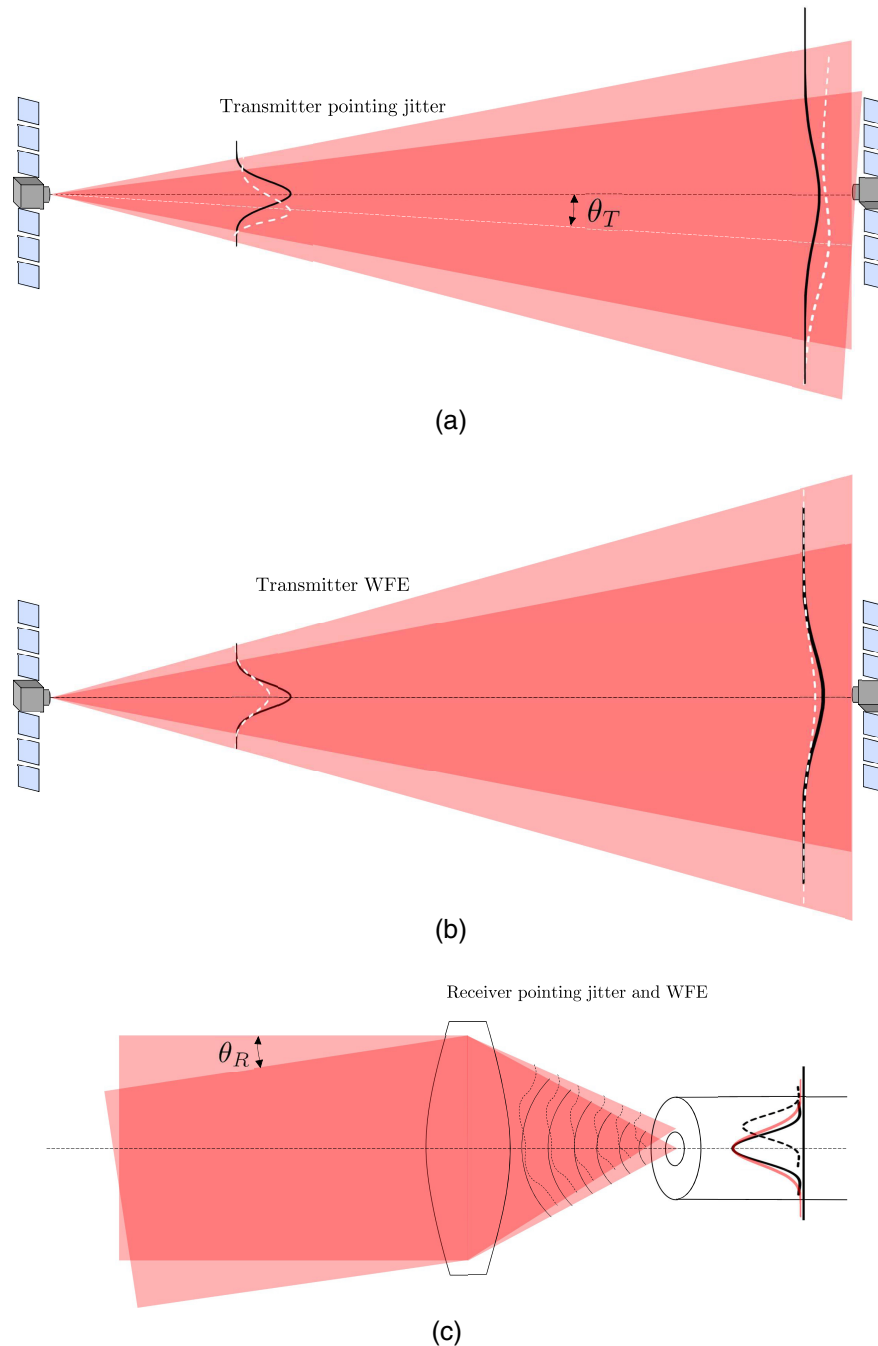
Fig. 12 Impact of opto-thermo-mechanical phenomena in FSOC: (a) transmitter pointing jitter: the white dashed-line and the black line are the intensity profile of the beam with and without pointing error, respectively. (b) Transmitter WFE: the white dashed-line and the black line are the intensity profile of the beam with and without WFE, respectively. (c) Receiver pointing jitter and WFE: the red line is the intensity profile of the mode of the fiber, the black dashed and continuous lines are the intensity profile of the focused light with and without WFE and pointing jitter, respectively.

considered as a plane wavefront. Under random vibrations, such as those experienced by the onboard optical terminal, θ_T will be characterized by a PDF [Eqs. (1) and (2)]. For a link using a Gaussian beam and under transmitter pointing jitter given by a Rayleigh PDF [Eq. (1)], the PDF of the intensity at the receiver aperture is described by a beta distribution:[104]

$$p(\mathcal{I}) = \beta \mathcal{I}^{(\beta-1)}, \quad \text{where } \beta = \frac{w_0^2}{4\sigma^2} \quad \text{for } 0 \leq \mathcal{I} \leq 1, \tag{8}$$

where w_0 is the beamwaist fo the Gaussian beam, $\mathcal{I}$ is the normalized intensity, and the average intensity is given by $I_{\text{avg}} = \beta/(\beta + 1)$. (This equation considers that the beamwidth of the beam in the aperture plane of the receiver is much larger than the receiver aperture size. In this way, the variation of the intensity across the aperture is negligible.) Therefore, the average intensity in the receiver's aperture can be obtained by combining the far field Fraunhofer diffraction intensity profile in the receiver's aperture plane and the PDF of the θ_T. Through this reduction of the average intensity of the signal, the SNR will decrease giving an increase in the BER. For different modulation techniques[105,106] and receiver architectures (direct or coherent),[71,107] different BER models will be used to compute the effect of transmitter pointing jitter in communication.

Furthermore, the pointing jitter will also affect the communication performance of multiplexed links. The transmitter's pointing jitter could create cross-talk between the signals multiplexed in the same beam. This effect is significant in OAM multiplexed links because of the spatial dependence of this multiplexing technique. The result of the transmitter pointing error in OAM multiplexed FSOC is discussed by Xie et al.[108] and Li et al.[109] In mode division multiplexed links, which makes use of other orthogonal beam modes (e.g., Hermite–Gaussian beams) to multiplex the signal, the transmitter pointing error can also be a potential source of crosstalk between the signals.[110]

5.2 Transmitter Wavefront Error

The WFE induced by the thermo-mechanical phenomena occur in both transmitter and receiver terminals. The WFE induced in the transmitter results in a decrease of the intensity at the aperture plane of the receiver and an increase in the beam divergence angle [Fig. 12(b)]. This effect can be quantified by propagating the field at the aperture of the transmitter to the aperture plane of the receiver through Fraunhofer's diffraction. Yang et al.[111] analyzed the impact of the transmitter WFE in an FSOC communication link using on–off keying modulation. This analysis shows that for the same root-mean-square value of the primary aberrations, coma aberration will have the largest impact while spherical aberration the least.

Requirements on the maximum WFE for FSOC are dependent on the specific link parameters but usually $\text{WFE}_{\text{rms}} < \lambda/30$ for the on-axis field of view and $\text{WFE}_{\text{rms}} < \lambda/15$ for the whole field of view are a good rule of thumb for a preliminary terminal design in the wavelengths used in FSOC.[102,112,113]

As explained in Sec. 3.2, the laser beam itself can induce thermo-elastic deformations in optical microcomponents without enough thermal sinking, such as the microelectromechanical mirrors.[66] This type of load will only occur in the transmitter terminal because the intensity of the received signal in the receiver will usually be orders of magnitudes below the one of the transmitter.

5.3 Receiver's Pointing Jitter

The receiver's pointing jitter (see Fig. 11) will create a random beam walk-off at the detector plane. The impact on the communication performance of this random beam walk-off will be dependent on the architecture of the receiving terminal. If the photodetector is sufficiently large that the focal spot radius is contained within it, then the degradation due to the random walk-off is negligible. When the detector is not big enough, then the effect on the intensity received can be computed through the degradation factor proposed by Zaman and Boyraz.[71] In fact, the pointing jitter in the detector will have the largest effect when the incoming link is coupled into an optic fiber onboard the receiver's terminal [see Fig. 12(c)].

When the communication system couples the receiving light to a fiber through a coupling lens, the pointing jitter will decrease the fiber-coupling efficiency. The instantaneous fiber coupling efficiency can be calculated in the presence of receiver pointing jitter, θ_R, for both single-mode[114] and multimode[115] fibers as

$$\eta_{C,mn} = \frac{P_C}{P_A} = \frac{\left| \iiint_A E_s(\theta_R, \rho, \phi) E_{mn}^*(\theta_T, \rho, \phi) p(\theta_R) \rho d\rho d\phi \, d\theta_R \right|^2}{\iint_A |E_s(\rho, \phi)|^2 \rho d\rho \, d\phi}, \tag{9}$$

where $\eta_{C,mn}$ is the coupling efficiency of the LP_{mn} mode (LP mode refers to the characteristic linearly polarized modes of the fiber-optic considered), P_C is the power coupled in the fiber, and

P_A is the total available power at the aperture of the coupling lens (considering negligible the transmission losses through the terminal, this is equal to the power available at the aperture of the receiver). E_s is the electric field in the focal plane, E_{mn} is the fiber mode corresponding to mode LP_{mn}, and $\{\rho, \phi\}$ are the polar coordinates at the fiber coupling plane. $p(\theta_R)$ is the PDF of the receiver's pointing jitter. This coupling efficiency can then be introduced to the Gaussian-Q function using the theory shown in Ref. 71 to obtain the BER. (Although this is not the kind of coupling considered in this paper, the rationale behind the approach is equivalent.)

When the link is OAM multiplexed the receiver's pointing jitter will also induce crosstalk between the multiplexed signals, similar to the case of the transmitter jitter.[108] The crosstalk in the case of the receiver's pointing jitter is due to a tilted phase added to the phase of the OAM multiplexed beam at the receiver plane.

5.4 Receiver's Wavefront Error

As for the WFE induced on the optical terminal of the receiver, the spot at the detector plane will increase in size and move its position. Usually, these two effects created by thermo-mechanical loads on the satellite are small enough that the spot remains contained within the detector.[69,111]

However, when the incoming beam is coupled into a fiber [see Fig. 12(c)], the WFE induced by the thermo-mechanical phenomena in the receiver terminal will decrease the coupling efficiency.[116,117] This effect can be computed by obtaining the field E_s in the focal plane of the fiber coupler in the presence of WFE in the receiver and using Eq. (9).

The overall effects in the communication performance due to all the phenomena presented above can be quantified for an on–off keying modulation scenario through the BER:[71,103]

$$\text{BER} = \int_0^\infty \int_0^\infty \frac{1}{2} \text{erfc}\left(\frac{Q(\theta_T, \text{WFE}_T, \theta_R, \text{WFE}_R, \mathbb{S})}{\sqrt{2}}\right) p(\theta_T) p(\theta_R) \mathrm{d}\theta_T \, \mathrm{d}\theta_R, \qquad (10)$$

where Q is the Gaussian-Q function, and $\mathbb{S}$ are the design parameters of both terminals. Therefore, all the effects presented above can be quantified through the Gaussian-Q factor defined as

$$Q(\theta_T, \text{WFE}_T, \theta_R, \text{WFE}_R, \mathbb{S}) = \frac{i_{D-1} - i_{D-0}}{\sigma_{N-1} + \sigma_{N-0}}, \qquad (11)$$

where $i_{D-1,0}$ is the instantaneous signal current at the detector and $\sigma_{N-1,0}$ is the noise variance for the 1 and 0 bits, respectively. The instantaneous signal current values are affected by the pointing jitters and WFE in both the transmitter and the receiver (therefore are dependent on the parameters $\{\theta_T, \text{WFE}_T, \theta_R, \text{WFE}_R, \mathbb{S}\}$, not explicitly shown in the equation above for simplification). The pointing jitter and the WFE of the transmitter will reduce the value of instantaneous signal current through the reduction of the power received at the aperture plane of the receiver. The pointing jitter of the receiver will reduce the signal current by affecting the degradation factor.[71] Finally, the WFE in the receiver will reduce the instantaneous current signal by a fiber coupling efficiency reduction.

5.5 Polarization Effects

As stated in Sec. 1, the polarization property of the laser beam can be exploited for communication purposes in FSOC. Therefore, changes in the polarization state due to stress birefringence can affect the performance of the link.[6,118] There are several devices (see Sec. 2) in FSOC terminals that can be affected by stress birefringence and therefore affect the polarization of the beam. The most susceptible component on a terminal to polarization effects is the PBS, which is used to split the incoming beam into two orthogonally polarized beams. In the presence of stress birefringence, crosstalk between the two output beams could occur due to a change in polarization induced by the stress field.[97] This could in turn yield several effects depending on the role polarization is playing in the communication link.

- If the beam is linearly polarized and to be used in a coherent detection system, then the changes in polarization due to stress birefringence (both in transmitter and receiver) will yield a reduction in the intensity received at the detector and therefore an increase in BER. In this case, an effort has to be made to ensure that the polarization is maintained within

Table 2 Optical performance parameters affected by opto-thermo-mechanical phenomena, along with their performance metric and a brief description of their effect on FSOC.

	Performance metrics	Effect on FSOC
Pointing errors	Angular pointing jitter PDF and σ^2 [see Eqs. (1) and (2)]	Transmitter pointing error decreases the signal on the receiver. Receiver pointing error changes the angle of incidence of the incoming beam creating a less efficient fiber coupling. Furthermore, in spatially multiplexed beams the pointing error creates crosstalk between the information channels
WFEs	Zernike coefficients of the WFE and WFE$_{rms}$	Transmitter WFE reduces the intensity in the far field in the axis of the beam. Receiver WFE reduces the fiber coupling efficiency. Furthermore, in spatially multiplexed beams WFEs create crosstalk between the information channels
Polarization effects	PER	Depending on the use of the polarization property, this could create a reduction in the received intensity, bit errors, or crosstalk

boundaries in the adverse space environment.[6] The maintenance of polarization required for this kind of link is quantified through the PER.

- If polarization modulation is used in the link, then the change in polarization will directly increase the BER due to the higher probability of receiving an erroneous bit value.
- If polarization division multiplexing is used in the link, then crosstalk between the signals multiplexed in the same beam could occur.

In this section, several optical performance parameters that are affected by opto-thermo-mechanical phenomena have been investigated. An overview of these parameters, the metrics used for their characterization, and a summary of their effects in FSOC are presented in Table 2.

6 Mitigation Techniques

The opto-thermo-mechanical phenomena in an FSOC satellite can greatly impact the communication performance as stated before. In order to diminish the impact of these phenomena, several mitigation techniques can be applied. In this section, a review of these techniques is presented.

The mitigation techniques are classified according to the source of the opto-thermo-mechanical phenomena (i.e., in-orbit microvibrations or thermal loads). It has been seen before that these sources could create similar opto-thermo-mechanical phenomena and therefore have an effect on the same optical performance parameters (see Fig. 1). On one hand, microvibrations will mainly create rigid body motions (of both satellite and components) and therefore pointing jitter, the mitigation techniques associated with these items is covered first. On the other hand, the thermal sources will mainly create surface deformations, stress birefringence, and thermo-optical dispersion. These will in turn give polarization effects and WFE of the system. Hence, the mitigation techniques related to these items are covered second.

6.1 Microvibrations

In order to reduce satellite microvibrations and diminish their detrimental effects on FSOC, mitigation techniques can be applied on several layers. The first layer includes reducing the microvibrations onboard by smart design of the attitude, determination, and control system (ADCS) and structural system of the satellite. These mitigation techniques are common to any satellite that require good pointing stability on their specific application (e.g., Earth observation and astronomy). Three different measures can be taken at this layer, classified according to where in the satellite the measure is applied.[119]

- *Microvibration source suppression*. The intensity of some of the internal microvibration sources listed in Sec. 3.1 can be suppressed or reduced by a proper design of the
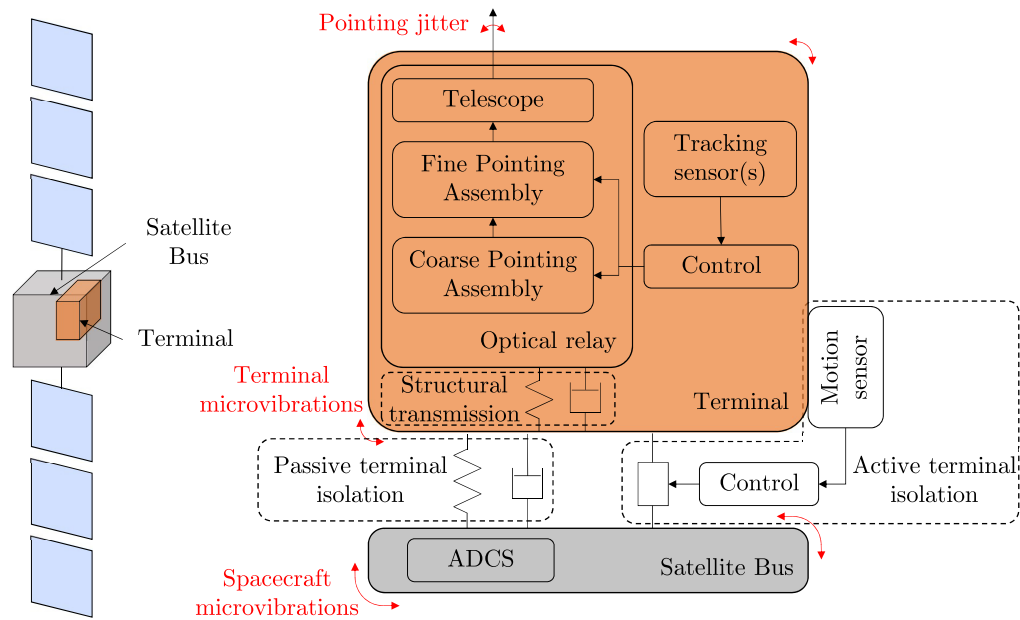
Fig. 13 FSOC satellite microvibration mitigation techniques. Microvibrations at different system levels of the satellite are represented through red arrows. ADCS system in the bus is depicted to represent one of the many possible onboard vibration sources.

systems involved as presented by Li et al.[119] Special attention must be dedicated to the reduction of the reaction wheel microvibrations as this is one of the main sources of microvibrations.[29,120] Furthermore, operational improvements can be made to suppress or reduce the intensity of these sources.[121] This could mean turning off some of the equipment or limiting the operation ranges of these whenever possible. The latter could be applied by not operating the satellite communication under the thermal snap induced microvibrations when entering or going out of the eclipse.

- *Terminal isolation*. As shown in Fig. 13, the terminal can be isolated through both passive and active isolators. A review of the techniques to isolate the optical terminal from the spacecraft microvibrations is presented by Liu et al.[122] The isolation techniques developed for other space-borne instruments can be transferred to FSOC systems. Hyde et al.[123] presented a specific example of the use of a passive hexapod isolation system for FSOC.

- *Structural transmission path suppression*. The microvibrations arriving at the payload will be transferred to the optical relay of the terminal as represented in Fig. 13. Through a detailed structural dynamics analysis[84] and the optimization of the optical mounts for the different components, the vibrations can be isolated on a component level through the transfer path suppression technique. The analysis of such a technique to design the supporting structure of a satellite FSOC telescope is presented by Nevin et al.[112] This mitigation technique can also be applied at a more general satellite level, for the design of the bus structure and the optimization of the location of the internal microvibration sources (e.g., reaction wheels and solar array drive mechanism).

Each of the microvibration suppression and isolation techniques described will have an effect on different frequency ranges of the PSD of the microvibration (see Fig. 5). Several examples of the different methods of suppression and isolation are presented in Table 3, stating the frequency ranges in which they will attenuate the PSD of the microvibration. High-frequency microvibrations, above 500 Hz, have a much lower influence on the pointing jitter and are usually suppressed by the structure itself (transmission path suppression).[124]

The second layer would be to use active correcting components on the optical terminal to compensate for microvibrations (i.e., CPA and FSM). An extensive survey of the available fine and coarse steering mechanisms that can be used in mobile FSOC terminals, such as a satellite terminal, is presented by Kaymak et al.[125] Different fine steering architectures are investigated by

Table 3 Spacecraft microvibration suppression methods and frequency ranges attenuated by them.[124]

	Low frequency (<5 Hz)	Mid frequency (5 to 500 Hz)
Source	Drag free technology, multifunctional attitude control	Fluid viscous damper, viscoelastic materials, magnetorheological damper, particle damper, tuned mass damper, metal rubber dumper, voice coil damper, piezoelectric hybrid damper, electromagnetic hybrid damper
Payload isolation	Drag free payload	Magnetic flux pinning
Transmission path	Metamaterial damper	Metamaterial damper

Miller et al.[126] and the impact of including a fine steering assembly in a satellite communication terminal is quantified in the satellite-to-ground experiment onboard Micius.[34] The terminal microvibration requirements can also be relaxed through the use of wide-field angle receivers.[127]

Finally, the mitigation of the impact of microvibrations on FSOC systems can be attained through the shaping and modulation of the laser beam itself. Beam size optimization can be used to reduce the impact of transmitter pointing jitter,[72,105,128,129] receiver pointing jitter,[114] or a combination of both.[130] The impact of the pointing jitter in different modulation techniques[105,107,131] and different terminal architectures[71] will determine the optimal combination of these to minimize the effects of pointing jitter in FSOC.

Other mitigation techniques that are not specific but can also attenuate the effects of microvibrations can be found in the literature.[1,132] The right combination of the previously presented mitigation techniques will enable the optimal design of the communication system.

6.2 Thermal Phenomena

The effects induced by thermal loads and their impact on an FSOC satellite can be mitigated in several ways. Given that the thermal loads will mainly create surface deformations, stress birefringence, and thermo-optic dispersion, the mitigation techniques related to reducing the WFE and polarization effects are considered in this section (considering the structure presented in Fig. 1). Depending on where the mitigation technique is implemented, these can be classified as follows.

- *Satellite thermal control*. Proper control of the external (see Fig. 6) and internal thermal loads on a satellite level can be achieved through different techniques.[46,133,134] Both active and passive thermal control mechanisms will help to obtain a more stable operation temperature environment for the terminal. Furthermore, the thermal management of internal heat loads is paramount when these loads are high (e.g., EDFA). An example of a passive thermal management technique onboard the TBIRD satellite terminal is done by placing the components that generate most of the heat close to the external faces of the enclosure, increasing their radiation to space.[64]

- *Component design and athermalization*. It is not possible to achieve a completely constant and uniform temperature in the satellite with the satellite-level thermal control techniques. Therefore, the optical mounts and components of the terminal must be carefully designed to reduce the mechanical stresses and deformations under the given thermal environment. In this way, the WFE and stress birefringence phenomena can be reduced. The stability of the optical performance of the terminal under the cyclic thermal space environment can be achieved by athermalizing optical components.[135] To do so different design parameters, such as geometry (flexures[136]), materials, and coatings (attending to their thermomechanical and thermo-optical properties) have to be combined to achieve the optimum solution.[112] A combination of these techniques is presented for a catadioptric telescope design for an FSOC satellite by Rahman et al.[137] and in the design of the FSOC TBIRD terminal.[65] A hermetic sealing of the mirror inside a container filled with inert gas has been proposed to create convection thermal transfer and mitigate the effects of thermal loads in a microelectromechanical FSM.[66]

- *WFE compensation*. The relative effect on the propagation of the transmitter WFE in different beam profiles will be different. In links where non-Gaussian beams are used for purposes, such as multiplexing[20] or atmospheric turbulence mitigation,[138] the link could also be more resilient to the effects of the transmitter WFE. In this way, the requirements for the WFE in the transmitter terminal could be relaxed. On-ground receiver terminals using adaptive optics systems to compensate for the atmospheric turbulence[116,139] can also correct for the WFE induced by opto-thermo-mechanical phenomena. In this way, the coupling efficiency can be increased when an optical fiber is used for the detection of the signal. Adaptive optics systems onboard satellites have also been proposed to correct for the aberrations produced in satellite FSOC terminals.[140]

- *Polarization compensation*. An active compensation in the receiver side to correct for polarization mode dispersion occurring in optical fibers is presented by Nabavi and Hall[141]. This method could be applied on optical coherent receivers to compensate for polarization mode dispersion created by opto-thermo-mechanical phenomena in FSOC.

The WFE and polarization compensation techniques should not be applied as the main solution to reduce the impact of these induced by opto-thermo-mechanical phenomena in the communication link. Instead, thermal control techniques and smart component design should be applied to reduce the WFE and the change in polarization state created by opto-thermo-mechanical phenomena.

7 Future Work

To improve the communication performance of FSOC, several challenges related to the opto-thermo-mechanical phenomena occurring in the optical terminals have to be studied.

The pointing accuracy of the transmitted beam is one of the key performance parameters on FSOC links. The classical solutions for steering the beam have been mainly based on mechanical PAT mechanisms, such as gimbals and FSMs. However, during the last years, non-mechanical beam steering systems have raised a lot of interest in the field due to their lower weight and bulkiness, and their extended operating lifetime.[142] Several non-mechanical beam steering mechanisms have been proposed for their application in FSOC.[143] There is a vast diversity of non-mechanical beam steering techniques, such as those based on liquid crystal devices,[144–146] optical phased arrays,[147] and focal plane switch array.[148] Furthermore, several techniques have been proposed to simultaneously steer and shape the beam combining the previous with variable focal lenses.[142,149] Further research is required to enable the use of these devices in FSOC terminals in space, especially regarding their performance and lifetime under the periodic temperature changes to which they would be exposed.

Some of the non-mechanical beam steering techniques presented above are based on integrated photonic circuits.[147] In fact, integrated photonic devices are currently being investigated for their application in FSOC. Especially in the space segment, FSOC terminals would hugely benefit from the multifunctionality and small size of these devices.[150,151] Many applications have been proposed for the use of integrated photonic devices in FSOC[152–154] and more specifically in spacecraft terminals.[155] The effects of radiation and thermal loads in space can be critical for the operation and lifetime of these components.[156,157] Furthermore, the optical powers onboard the satellites can sometimes be too high for integrated waveguides due to non-linear effects.[155] Further research on the radiation hardness and the thermal management of these devices will be key for their implementation in FSOC satellite terminals.

As it has been mentioned in Sec. 6, adaptive optics systems could be used to compensate WFE due to opto-thermo-mechanical phenomena onboard satellites. On one hand, adaptive optics systems in space to correct perturbations due to opto-thermo-mechanical phenomena[158] have been studied in depth for their application in astronomical telescopes.[159–162] On the other hand, adaptive optics have been widely used in the ground segment of FSOC systems during the last decades for correcting atmospheric distortions.[163] However, little research has been done on the use of adaptive optics systems onboard FSOC satellite terminals,[140] to compensate for WFE generated by both atmospheric and opto-thermo-mechanical phenomena.

The benefits of mechanical metamaterials for vibration isolation can be exploited in space applications in the future.[164] Periodic macroscopic lattice cell structures can be customized with

the aid of additive manufacturing to obtain the desired vibration mitigation characteristics. Combining the design flexibility with the low mass, the use of these metamaterials seems to be promising for satellites using FSOC. Studies on the applicability of these to FSOC satellites and their qualification for the space environment should be investigated in the coming years.[165]

Due to their versatility and low mass, diffractive optical elements have been proposed for FSOC for signal multiplexing,[166,167] multibeam transmitter design,[168] system size reduction,[169,170] and beam spot size reduction.[171] Although athermalization of diffractive elements has been investigated previously,[172,173] a better understanding of the opto-thermo-mechanical phenomena in this type of component is required to be used in FSOC satellite terminals.

Similar to diffractive optics, metasurfaces have shown to have several benefits compared to classical refractive and reflective optics used generally in FSOC.[174] The metasurface technology is maturing rapidly and will enable a lot of new possibilities for FSOC, e.g., compact wide field angle receivers[175] and multiplexing.[176,177] The opto-thermo-mechanical behavior of these components and their impact on communication has to be further understood to extend their applicability to satellite terminals in the future. Some opto-thermo-mechanical phenomena occurring in metasurfaces have already been investigated in mechanically[178,179] and thermally[180] tunable metasurfaces.

Considering the impact of the pointing jitter, WFE, and polarization on the communication link, several research gaps relevant to this work have been identified.

- The impact of pointing jitter and WFE on links with different modulation techniques has to be methodologically assessed. As a result, the optimum combination of the requirements on satellite microvibrations and WFE for different modulation techniques can be derived.
- The combined effect of pointing jitter and WFE on the propagation of different beam shapes (e.g., Hermite–Gaussian, Laguerre–Gaussian, and Top Hat) has to be assessed.

As has been discussed in the previous section, microvibration suppression on satellite FSOC terminals is key for increasing the performance of the link. The application of novel microvibration mitigation techniques has to be applied to satellite FSOC terminals, these include drag-free devices, voice coil dampers, and magnetic flux pinning. Some of the problems that should be investigated in the future regarding microvibration suppression are presented by Jiao et al.[124]

In a similar manner, spacecraft thermal management methods and their use in satellite FSOC have to be further investigated. Recent advances in spacecraft thermal control have been significant in both passive and active devices.[181,182] Research on passive components includes phase change materials for heat storage to reduce radiator size,[183] materials, such as graphene and aerosols,[184] and multifunctional nanostructure surfaces that modulate the emissivity and absorptivity to optimize the thermal performance.[185] Miniaturization of active thermal devices, such as cryocoolers[181] and pumped fluid loops for small satellites,[186] will be also relevant for future FSOC systems.

8 Summary

The role of opto-thermo-mechanical phenomena in FSOC and their impact on communication on satellite terminals have been described in this paper. The characterization of the thermal and mechanical environment to which the terminals are subjected has been explained. The opto-thermo-mechanical phenomena created by these loads on FSOC terminals and how to model them have also been described. These phenomena include satellite rigid body displacements and rigid body motion, surface deformation, thermal dispersion, and stress birefringence of the optical components. The impact of these phenomena on the communication link has been described by categorizing according to where these occur (i.e., transmitter or receiver). Furthermore, the changes in the state of polarization due to the opto-thermo-mechanical phenomena have also been assessed.

Several mitigation techniques to reduce the effects on the optical performance of the terminal, and to diminish the impact on the link have also been presented. Finally, research challenges that exist for the development of future FSOC terminals have been identified.

Further investigation on the topics covered in Sec. 7 will be essential to the development of future satellite FSOC.

Code, Data, and Materials Availability

Acknowledgments

References

1. H. Kaushal and G. Kaddoum, "Optical communication in space: challenges and mitigation techniques," *IEEE Commun. Surv. Tutorials* **19**, 57–96 (2017).
2. A. Jahid, M. H. Alsharif, and T. J. Hall, "A contemporary survey on free space optical communication: potentials, technical challenges, recent advances and research direction," *J. Netw. Comput. Appl.* **200**, 103311 (2022).
3. A. Könsgen and A. Förster, "Current state and future challenges in deep space communication: a survey," *Inf. Technol.* **63**(4), 219–234 (2021).
4. H. Hemmati, A. Biswas, and I. B. Djordjevic, "Deep-space optical communications: future perspectives and applications," *Proc. IEEE* **99**, 2020–2039 (2011).
5. A. Vats, H. Kaushal, and V. Jain, "Free space optical communication: laser sources, modulation schemes and detection techniques," in *IEEE Int. Conf. Telecommun. and Networks (TEL-NET-2013)* (2013).
6. M. Dinu et al., "Qualification and performance of a high-efficiency laser transmitter for deep-space optical communications," *Proc. SPIE* **11993**, 119930G (2022).
7. W. Shao et al., "Terabit FSO communication based on a soliton microcomb," *Photonics Res.* **10**, 2802–2808 (2022).
8. A. Bekkali, H. Fujita, and M. Hattori, "New generation free-space optical communication systems with advanced optical beam stabilizer," *J. Lightwave Technol.* **40**, 1509–1518 (2022).
9. A. Turpin et al., "Free space optical polarization de-multiplexing and multiplexing by means of conical refraction," *Opt. Lett.* **37**, 4197–4199 (2012).
10. S. Benedetto and P. Poggiolini, "Theory of polarization shift keying modulation," *IEEE Trans. Commun.* **40**, 708–721 (1992).
11. X. Tang et al., "Free-space optical communication employing polarization shift keying coherent modulation in atmospheric turbulence channel," in *7th Int. Symp. Commun. Syst., Networks & Digital Signal Process. (CSNDSP 2010)*, pp. 615–620 (2010).
12. R. Zhang et al., "4 × 100-Gb/s PAM-4 FSO transmission based on polarization modulation and direct detection," *IEEE Photonics Technol. Lett.* **31**, 755–758 (2019).
13. Y. Zhao et al., "Circular polarization shift-keying modulation based on orbital angular momentum division multiplexing in free space optical communication," *Opt. Commun.* **475**, 126165 (2020).
14. Z.-Y. Chen et al., "Use of polarization freedom beyond polarization-division multiplexing to support high-speed and spectral-efficient data transmission," *Light Sci. Appl.* **6**, e16207–e16207 (2017).
15. J. Wu et al., "Polarization-maintaining design for satellite-based quantum communication terminals," *Opt. Express* **28**, 10746–10759 (2020).
16. K. B. Doyle et al., "Stress birefringence modeling for lens design and photonics," *Proc. SPIE* **4832**, 436–447 (2002).
17. H. Hemmati, *Near-Earth Laser Communications*, CRC Press (2009).
18. A. M. Yao and M. J. Padgett, "Orbital angular momentum: origins, behavior and applications," *Adv. Opt. Photonics* **3**, 161–204 (2011).
19. G. Gibson et al., "Free-space information transfer using light beams carrying orbital angular momentum," *Opt. Express* **12**, 5448–5456 (2004).
20. A. E. Willner et al., "Orbital angular momentum beams for high-capacity communications," *J. Lightwave Technol.* 41, 1918–1933 (2022).
21. B. Naimullah et al., "Comparison of wavelength propagation for free space optical communications," in *Int. Conf. Electron. Des.*, pp. 1–5 (2009).

22. T. Plank et al., "Wavelength-selection for high data rate Free Space Optics (FSO) in next generation wireless communications," in *17th Eur. Conf. Networks and Opt. Commun.*, pp. 1–5 (2012).

23. R. Miglani, "Analysis of FSO communication links for mid and far infrared wavelengths," *Int. J. Sci. Eng. Res.* **4**(7), 5 (2013).

24. T. Liu et al., "Investigation of the wavelength selection for the free space optical communication system," in *Asia Commun. and Photonics Conf. (ACP)*, pp. 1–3 (2018).

25. Y. Lu et al., "A review of the space environment effects on spacecraft in different orbits," *IEEE Access* **7**, 93473–93488 (2019).

26. F. Berghmans et al., "An introduction to radiation effects on optical components and fiber optic sensors," in *Optical Waveguide Sensing and Imaging*, W. J. Bock, I. Gannot, and S. Tanev, Eds., pp. 127–165, Springer, Dordrecht (2007).

27. S. Girard et al., "Recent advances in radiation-hardened fiber-based technologies for space applications," *J. Opt.* **20**, 093001 (2018).

28. S. Arnon and N. Kopeika, "Laser satellite communication network-vibration effect and possible solutions," *Proc. IEEE* **85**, 1646–1661 (1997).

29. C. Dennehy and O. S. Alvarez-Salazar, "A survey of the spacecraft line-of-sight jitter problem," in *AAS Annu. Guidance and Control Conf.* (2019).

30. L. You et al., "Superconducting nanowire single photon detection system for space applications," *Opt. Express* **26**, 2965–2971 (2018).

31. N. Jedrich et al., "Cryo cooler induced microvibration disturbances to the Hubble Space Telescope," NASA STI/Recon Technical Report N (2002).

32. D. Yu, G. Wang, and Y. Zhao, "On-orbit measurement and analysis of the micro-vibration in a remote-sensing satellite," *Adv. Astron. Sci. Technol.* **1**, 191–195 (2018).

33. X. Tang et al., "Overview of Earth observation satellite platform microvibration detection methods," *Sensors* **20**, 736 (2020).

34. X. Wang et al., "Angular micro-vibration of the Micius satellite measured by an optical sensor and the method for its suppression," *Appl. Opt.* **60**, 1881–1887 (2021).

35. M. E. Wittig et al., "In-orbit measurements of microaccelerations of ESA's communication satellite Olympus," *Proc. SPIE* **1218**, 205–214 (1990).

36. M. Toyoshima et al., "In-orbit measurements of spacecraft microvibrations for satellite laser communication links," *Opt. Eng.* **49**, 083604 (2010).

37. M. Toyoshima and K. Araki, "In-orbit measurements of short term attitude and vibrational environment on the Engineering Test Satellite VI using laser communication equipment," *Opt. Eng.* **40**, 827–832 (2001).

38. S. Dyne, P. Collins, and D. Tunbridge, "Satellite mechanical health monitoring," in *IEE Colloq. Adv. Vibr. Meas., Tech. and Instrum. for the Early Predict. of Failure*, pp. 4/1–4/8 (1992).

39. S. Dyne, D. Tunbridge, and P. Collins, "The vibration environment on a satellite in orbit," in *IEE Colloq. High Accuracy Platform Control in Space*, pp. 12/1–12/6 (1993).

40. J. Johnston and E. Thornton, "Thermally induced dynamics of satellite solar panels," *J. Spacecr. Rockets* **37**, 604–613 (2000).

41. M. Oda et al., "Measurement of satellite solar array panel vibrations caused by thermal snap and gas jet thruster firing," in *Recent Advances in Vibrations Analysis*, N. Baddour, Ed., IntechOpen (2011).

42. D. González-Bárcena et al., "Selection of time-dependent worst-case thermal environmental conditions for Low Earth Orbit spacecrafts," *Adv. Space Res.* **70**, 1847–1868 (2022).

43. J. Hansen et al., "Earth's energy imbalance and implications," *Atmos. Chem. Phys. Discuss.* **11**, 13421–13449 (2011).

44. Copernicus Climate Change Service, "Surface albedo 10-daily gridded data from 1981 to present," 2018, Copernicus Climate Change Service (C3S) Climate Data Store (CDS) (accessed 1 January 2023).

45. Copernicus Climate Change Service, "Earth's radiation budget from 1979 to present derived from satellite observations," Copernicus Climate Change Service (C3S) Climate Data Store (CDS) (accessed 1 January 2023).

46. D. G. Gilmore, *Spacecraft Thermal Control Handbook. Volume I, Fundamental Technologies*, 2nd ed., Aerospace Press (2002).

47. R. Jimenez, "Effects of natural environment charged particle heating on the design and performance of spacecraft cryogenic components," in *24th Thermophys. Conf., Fluid Dyn. and Co-Located Conf.*, American Institute of Aeronautics and Astronautics (1989).

48. H. Dang et al., "Development of 2-K space cryocoolers for cooling the superconducting nanowire single photon detector," *IEEE Trans. Appl. Supercond.* **29**, 1–4 (2019).

49. D. Hengeveld et al., "Hot and cold-case orbits for robust thermal control," *J. Spacecr. Rockets* **46**, 1249–1260 (2009).

50. B. J. Anderson, C. G. Justus, and G. W. Batts, "Guidelines for the selection of near-Earth thermal environment parameters for spacecraft design," Tech. Rep. NASA/TM–2001-211221 (2001).

51. C. G. Justus et al., "Simple Thermal Environment Model (STEM) user's guide," Tech. Rep. NAS 1.15:211222, NTRS Research Center: Marshall Space Flight Center (MSFC) (2001).

52. L. Yenchesky et al., "Optomechanical design for CubeSat laser infrared crosslinks," in *AIAA Scitech 2019 Forum* (2019).

53. H. Zhang et al., "On-orbit thermal deformation prediction for a high-resolution satellite camera," *Appl. Therm. Eng.* **195**, 117152 (2021).

54. S.-P. Chen, "Investigations of free space and deep space optical communication scenarios," *CEAS Space J.* **14**(2), 357–364 (2022).

55. C. E. DeVoe et al., "Optical overview and qualification of the LLCD space terminal," *Proc. SPIE* **10563**, 105630F (2017).

56. A. Biswas, D. Boroson, and B. Edwards, "Mars laser communication demonstration: what it would have been," *Proc. SPIE* **6105**, 610502 (2006).

57. W. Hart et al., "Requirements development and management on the psyche project," in *IEEE Aerosp. Conf.*, pp. 1–14 (2019).

58. C. Y. Han and J.-M. Choi, "Thermal analysis of spacecraft propulsion system and its validation," *KSME Int. J.* **18**, 847–856 (2004).

59. V. Ashoori et al., "Heat generation and removal in solid state," in *An Overview of Heat Transfer Phenomena*, S. N. Kazi, Ed., IntechOpen (2012).

60. H. Noda et al., "Thermal analyses for initial operations of the soft x-ray spectrometer onboard the Hitomi satellite," *J. Astron. Telesc. Instrum. Syst.* **4**, 011202 (2017).

61. A. Carrasco-Casado et al., "Development and space-qualification of a miniaturized CubeSat's 2-W EDFA for space laser communications," *Electronics* **11**, 2468 (2022).

62. E. Haddad et al., "Space qualification of a 10W single-mode PM optical amplifiers in the 1.5-μm region," *Proc. SPIE* **11852**, 118521Y (2021).

63. C. Campanella et al., "Theoretical investigation of thermal effects in high power Er^{3+}/Yb^{3+}-codoped double-clad fiber amplifiers for space applications," *Physica Status Solidi A* **216**(3), 1800582 (2019).

64. C. M. Schieler et al., "200 Gbps TBIRD CubeSat downlink: pre-flight test results," *Proc. SPIE* **11993**, 119930P (2022).

65. K. Riesing et al., "Pointing, acquisition, and tracking for the TBIRD CubeSat mission: system design and pre-flight results," *Proc. SPIE* **11993**, 119930Q (2022).

66. P. do Vale Pereira, M. T. Hunwardsen, and K. L. Cahoy, "Characterization of laser thermal loading on microelectromechanical systems-based fast steering mirror in vacuum," *Opt. Eng.* **59**, 056109 (2020).

67. P. L. Rall et al., "Simulation and compensation of thermal lensing in optical systems," *Opt. Express* **30**, 38643–38662 (2022).

68. K. Dobek, "Thermal lensing: outside of the lasing medium," *Appl. Phys. B* **128**, 18 (2022).

69. Y. Yang, G. Cao, and H. Zhao, "Influence of localized distortion in lenses on Strehl ratio in lasercom," *Optik* **124**, 6415–6418 (2013).

70. A. Calvi et al., *ECSS-E-HB-32-26A Spacecraft Mechanical Loads Analysis Handbook*, European Cooperation for Space Standardization (2013).

71. I. U. Zaman and O. Boyraz, "Impact of receiver architecture on small satellite optical link in the presence of pointing jitter," *Appl. Opt.* **59**, 10177–10184 (2020).

72. M. Toyoshima et al., "Optimum divergence angle of a Gaussian beam wave in the presence of random jitter in free-space laser communication systems," *J. Opt. Soc. Am. A* **19**, 567–571 (2002).

73. F. Yang, J. Cheng, and T. A. Tsiftsis, "Free-space optical communication with nonzero boresight pointing errors," *IEEE Trans. Commun.* **63**, 713–725 (2014).

74. F. D. Iv and G. Nadorff, "Rigid body movements of optical elements due to opto-mechanical factors," *Proc. SPIE* **5867**, 58670H (2005).

75. V. L. Genberg, G. J. Michels, and K. B. Doyle, "Integrated modeling of jitter MTF due to random loads," *Proc. SPIE* **8127**, 81270H (2011).

76. S.-B. Chen et al., "Simulating and testing microvibrations on an optical satellite using acceleration sensor-based jitter measurements," *Sensors* **19**, 1797 (2019).

77. K. B. Doyle, "Structural line-of-sight jitter analysis for MLCD," *Proc. SPIE* **6665**, 66650I (2007).

78. P. Klocek, *Handbook of Infrared Optical Materials*, Optical Engineering, Vol. **30**, CRC Press, New York (1991).

79. S. Appel and J. Wijker, *Simulation of Thermoelastic Behaviour of Spacecraft Structures: Fundamentals and Recommendations*, Springer Nature (2021).

80. H.-S. Yang et al., "Three-shell-based lens barrel for the effective athermalization of an IR optical system," *Appl. Opt.* **50**, 6206–6213 (2011).

81. E. Segato et al., "Method for studying the effects of thermal deformations on optical systems for space application," *Appl. Opt.* **50**, 2836–2845 (2011).

82. K. B. Doyle et al., *Integrated Optomechanical Analysis* (2012).

83. C. B. Burroughs, R. W. Fischer, and F. R. Kern, "An introduction to statistical energy analysis," *J. Acoust. Soc. Am.* **101**, 1779–1789 (1997).

84. M. Remedia and G. Aglietti, "Modeling micro-vibrations transmission in spacecraft structures," in *62nd Int. Astron. Congr. 2011, IAC 2011*, Vol. 7, pp. 5682–5690 (2011).

85. R. M. Waxler and G. Cleek, "The effect of temperature and pressure on the refractive index of some oxide glasses," *J. Res. Natl. Bur. Stand., Sect. A* **77A**, 755 (1973).

86. Y.-F. Tsay, B. Bendow, and S. S. Mitra, "Theory of the temperature derivative of the refractive index in transparent crystals," *Phys. Rev. B* **8**, 2688–2696 (1973).

87. G. Ghosh, "Model for the thermo-optic coefficients of some standard optical glasses," *J. Non-Cryst. Solids* **189**, 191–196 (1995).

88. T. Bååk, "Thermal coefficient of refractive index of optical glasses," *J. Opt. Soc. Am.* **59**, 851–857 (1969).

89. C. J. Parker and W. A. Popov, "Experimental determination of the effect of temperature on refractive index and optical path length of glass," *Appl. Opt.* **10**, 2137–2143 (1971).

90. J. R. Rogers, "Passive athermalization: required accuracy of the thermo-optical coefficients," *Proc. SPIE* **9293**, 92931A (2014).

91. G. Michels and V. Genberg, "Analysis of thermally loaded transmissive optical elements," *Proc. SPIE* **8127**, 81270K (2011).

92. Y. C. Yiu and A. R. Meyer, "Computation of optical errors in transparent optical elements due to three-dimensional photoelastic effect," *Proc. SPIE* **1303**, 206–216 (1990).

93. E. Collett, *Field Guide to Polarization*, SPIE Press (2005).

94. E. Cotte et al., "Study of stress birefringence for 193-nm immersion photomasks," *Proc. SPIE* **5853**, 10–19 (2005).

95. H. Xiao and Z. Fan, "Imaging quality evaluation of aerodynamically heated optical dome using ray tracing," *Appl. Opt.* **49**, 5049–5058 (2010).

96. M. Huang, "Stress effects on the performance of optical waveguides," *Int. J. Solids Struct.* **40**, 1615–1632 (2003).

97. K. B. Doyle and W. M. Bell, "Thermo-elastic wavefront and polarization error analysis of a telecommunication optical circulator," *Proc. SPIE* **4093**, 18–27 (2000).

98. V. Genberg, G. Michels, and B. Myer, "Integrating optical, mechanical, and test software (with applications to freeform optics)," *Proc. SPIE* **10448**, 104480T (2017).

99. J. Moreno Raso et al., "Optomechanical design of the Laser Launch Telescope for the GTC adaptive optics system," *Proc. SPIE* **11871**, 1187109 (2021).

100. A. Haber et al., "Modeling and system identification of transient STOP models of optical systems," *Opt. Express* **28**, 39250 (2020).

101. J. Heijmans, M. Müller, and R. Holzlohner, "Combined Opto-mechanical analysis for modern optical instruments," *Proc. SPIE* **10705**, 107052D (2018).

102. D. Driscoll et al., "Deep space optical communications (DSOC) beam expander design and engineering," *Proc. SPIE* **11272**, 112720H (2020).

103. C.-C. Chen and C. Gardner, "Impact of random pointing and tracking errors on the design of coherent and incoherent optical intersatellite communication links," *IEEE Trans. Commun.* **37**, 252–260 (1989).

104. K. Kiasaleh, "On the probability density function of signal intensity in free-space optical communications systems impaired by pointing jitter and turbulence," *Opt. Eng.* **33**, 3748–3757 (1994).

105. H. Trung, "Performance of UAV-to-ground FSO communications with APD and pointing errors," *Appl. Syst. Innov.* **4**, 65 (2021).

106. K. Peppas and C. Datsikas, "Average symbol error probability of general-order rectangular quadrature amplitude modulation of optical wireless communication systems over atmospheric turbulence channels," *IEEE/OSA J. Opt. Commun. Networking* **2**, 102–110 (2010).

107. T. Song et al., "Impact of pointing errors on the error performance of intersatellite laser communications," *J. Lightwave Technol.* **35**, 3082–3091 (2017).

108. G. Xie et al., "Performance metrics and design considerations for a free-space optical orbital-angular-momentum–multiplexed communication link," *Optica* **2**, 357–365 (2015).

109. L. Li et al., "Orbital-angular-momentum-multiplexed free-space optical communication link using transmitter lenses," *Appl. Opt.* **55**, 2098–2103 (2016).

110. X. Liu et al., "Propagation characteristics of Hermite–Gaussian beam under pointing error in free space," *Photonics* **9**, 478 (2022).

111. Y. Yang et al., "Influence of wave-front aberrations on bit error rate in inter-satellite laser communications," *Opt. Commun.* **284**, 3065–3069 (2011).

112. K. E. Nevin, K. B. Doyle, and A. D. Pillsbury, "Optomechanical design and analysis for the LLCD space terminal telescope," *Proc. SPIE* **8127**, 81270G (2011).

113. D. Zhao et al., "Optimization design and performance test of optical antenna for laser communication," *Proc. SPIE* **10840**, 1084017 (2019).

114. M. Toyoshima, "Maximum fiber coupling efficiency and optimum beam size in the presence of random angular jitter for free-space laser systems and their applications," *J. Opt. Soc. Am. A* **23**, 2246–2250 (2006).

115. Y. Chen et al., "Coupling efficiency of a plane wave to few-mode fiber in the presence of beam random angular jitter," *J. Opt. Soc. Am. B* **38**, F8–F15 (2021).

116. W. Liu et al., "Free space optical communication performance analysis with focal plane based wavefront measurement," *Opt. Commun.* **309**, 212–220 (2013).

117. Y. Liu et al., "The effect of spatial mode distribution on coupling efficiency of single-mode fiber: theoretical analysis and experimental verification," *Appl. Sci.* **9**, 3296 (2019).

118. X. Xue et al., "Thermal vacuum optical performance test system for space laser communication terminal," *Proc. SPIE* **11052**, 1105215 (2019).

119. L. Li et al., "Micro-vibration suppression methods and key technologies for high-precision space optical instruments," *Acta Astronaut.* **180**, 417–428 (2021).

120. T. Hughes et al., "Design optimization of reaction wheel assembly characteristics to reduce spacecraft vibrations," in *AIAA SciTech Forum* (2022).

121. C. Dennehy and O. S. Alvarez-Salazar, "Spacecraft micro-vibration: a survey of experiences, potential solutions, and some lessons learned," Technical Memorandum 20180006315 (2018).

122. C. Liu et al., "Recent advances in micro-vibration isolation," *Mech. Syst. Sig. Process.* **56-57**, 55–80 (2015).

123. T. T. Hyde and L. P. Davis, "Vibration reduction for commercial optical intersatellite communication links," *Proc. SPIE* **3329**, 94–105 (1998).

124. X. Jiao et al., "Advances in spacecraft micro-vibration suppression methods," *Prog. Aerosp. Sci.* **138**, 100898 (2023).

125. Y. Kaymak et al., "A survey on acquisition, tracking, and pointing mechanisms for mobile free-space optical communications," *IEEE Commun. Surv. Tutor.* **20**(2), 1104–1123 (2018).

126. E. Miller et al., "Fine pointing and tracking concepts for optical intersatellite links," in *IEEE Int. Conf. Space Opt. Syst. and Appl. (ICSOS)*, pp. 208–213 (2017).

127. M. S. Islam and O. Boyraz, "Large aperture and wide field of view meta-receiver for free space optical communications," in *Conf. Lasers and Electro-Opt.*, Optica Publishing Group (2022).

128. A. A. Farid and S. Hranilovic, "Outage capacity optimization for free-space optical links with pointing errors," *J. Lightwave Technol.* **25**, 1702–1710 (2007).

129. P. X. Do et al., "Numerical and analytical approaches to dynamic beam waist optimization for LEO-to-GEO laser communication," *OSA Contin.* **3**, 3508–3522 (2020).

130. V. Mai and H. Kim, "Beam size optimization and adaptation for high-altitude airborne free-space optical communication systems," *IEEE Photonics J.* **11**, 7902213 (2019).

131. S. Arnon, S. R. Rotman, and N. S. Kopeika, "Performance limitations of free-space optical communication satellite networks due to vibrations: direct-detection digital mode," *Proc. SPIE* **3110**, 357–368 (1997).

132. A. K. Majumdar, *Advanced Free Space Optics (FSO): A Systems Approach*, Springer Series in Optical Sciences, Vol. **186**, Springer, New York (2015).

133. J. Miao et al., *Spacecraft Thermal Control Technologies*, Space Science and Technologies, Springer, Singapore (2021).

134. J. Meseguer, I. Pérez-Grande, and A. Sanz-Andrés, *Spacecraft Thermal Control*, Elsevier (2012).

135. M. Lesniewski and T. Kryszczynski, "Athermalization of optical systems," *Proc. SPIE* **3320**, 297–306 (1998).

136. A. Ahmad, *Handbook of Optomechanical Engineering*, CRC Press (2017).

137. S. K. S.-U. Rahman et al., "High performance all metal telescope for satellite based laser communication terminals," *Proc. SPIE* **12121**, 121210G (2022).

138. H. T. Eyyuboglu, C. Arpali, and Y. K. Baykal, "Flat topped beams and their characteristics in turbulent media," *Opt. Express* **14**, 4196–4207 (2006).

139. N. Kumar and V. Khandelwal, "Compensation of wavefront aberration using oppositional-breeding artificial fish swarm algorithm in free space optical communication," *J. Opt.* **52**, 1370–1380 (2022).

140. R. E. Morgan et al., "On-orbit operations summary for the Deformable Mirror Demonstration Mission (DeMi) CubeSat," *Proc. SPIE* **12185**, 121857O (2022).

141. N. Nabavi and T. J. Hall, "Symmetric signal and local oscillator polarization diverse coherent optical receiver," *Opt. Express* **24**, 2391–2405 (2016).

142. V. V. Mai and H. Kim, "Non-mechanical beam steering and adaptive beam control using variable focus lenses for free-space optical communications," *J. Lightwave Technol.* **39**, 7600–7608 (2021).

143. P. F. McManamon and A. Ataei, "Progress and opportunities in optical beam steering," *Proc. SPIE* **10926**, 1092610 (2019).

144. Z. Wang et al., "Liquid crystal spatial light modulator based non-mechanical beam steering system fractional-order model," *Opt. Express* **30**, 12178–12191 (2022).

145. H. Guo et al., "Research review on the development of liquid crystal optical phased array device on the application of free space laser communication," *Proc. SPIE* **10841**, 108410C (2019).

146. M. V. Gorkunov et al., "Non-mechanical multiplexed beam-steering elements based on double-sided liquid crystal metasurfaces," *Photonics* **9**, 986 (2022).

147. R. Mahon et al., "Two dimensional thermo-optic beam steering using a silicon photonic optical phased array," *Proc. SPIE* **9739**, 97390R (2016).

148. D. A. Goldman et al., "MOEMS-based lens-assisted beam steering for free-space optical communications," *J. Lightwave Technol.* **41**, 2675–2690 (2023).

149. F. Ishola et al., "Conceptual design and analysis of a compact liquid crystal on silicon non-mechanical optical beam steering antenna for lean platforms," *Proc. SPIE* **12413**, 124130N (2023).

150. Z. Wang et al., "On-chip integration of metasurface-doublet for optical phased array with enhanced beam steering," *Nanophotonics* **12**, 697 (2023).

151. D. Renner et al., "Integrated photonics technologies for sensing and free space communication," in *Appl. of Lasers for Sens. and Free Sp. Commun.*, Optica Publishing Group, p. LW3B.2 (2019).

152. C.-Y. Hsu, G.-Z. Yiu, and Y.-C. Chang, "Free-space applications of silicon photonics: a review," *Micromachines* **13**, 990 (2022).

153. V. Billault et al., "Robust free space optical communication receiver based on a spatial mode demultiplexer and a silicon photonic coherent combining circuit," *Proc. SPIE* **11993**, 1199304 (2022).

154. M. Milanizadeh et al., "Separating arbitrary free-space beams with an integrated photonic processor," *Light Sci. Appl.* **11**, 197 (2022).

155. G. N. Tzintzarov, S. G. Rao, and J. D. Cressler, "Integrated silicon photonics for enabling next-generation space systems," *Photonics* **8**, 131 (2021).

156. S. Piacentini et al., "Space qualification of ultrafast laser-written integrated waveguide optics," *Laser Photonics Rev.* **15**(2), 2000167 (2021).

157. R. T. Logan and D. Basuita, "Photonic components for spacecraft fiber optic datalinks and free-space optical communications terminals," *Proc. SPIE* **11852**, 1185244 (2021).

158. V. V. Corbacho, H. Kuiper, and E. Gill, "Review on thermal and mechanical challenges in the development of deployable space optics," *J. Astron. Telesc. Instrum. Syst.* **6**, 010902 (2020).

159. N. Devaney, "Active optics for space telescopes," in *Opt. Des. and Fabric. 2019 (Freeform, OFT) (2019)*, Optica Publishing Group, p. OW4A.4 (2019).

160. N. Devaney et al., "Development of a prototype active optics system for future space telescopes," *Appl. Opt.* **57**, E101–E106 (2018).

161. M. Laslandes et al., "Mirror actively deformed and regulated for applications in space: design and performance," *Opt. Eng.* **52**, 091803 (2013).

162. D. Grosse, F. Bennet, and M. Copeland, "Adaptive optics for satellite imaging and earth based space debris manoeuvres," in *Proc. 7th Eur. Conf. Space Debris, Darmstadt, Germany*, ESA Space Debris Office (2017).

163. X. Ke and P. Wu, *Adaptive Optics Theory and Its Application in Optical Wireless Communication, 237*, 1st ed., 2022 edition, Springer (2022).

164. M. Al Rifaie, H. Abdulhadi, and A. Mian, "Advances in mechanical metamaterials for vibration isolation: a review," *Adv. Mech. Eng.* **14**, 16878132221082872 (2022).

165. J. Y. Yoon, W. K. Song, and N.-C. Park, "Pendulum-type elastic metamaterial for reducing the vibration of a space tether," *Acta Astronaut.* **162**, 359–366 (2019).

166. G. Ruffato et al., "Test of mode-division multiplexing and demultiplexing in free-space with diffractive transformation optics," *Opt. Express* **25**, 7859–7868 (2017).

167. S. V. Karpeev et al., "Free-space transmission and detection of variously polarized near-IR beams using standard communication systems with embedded singular phase structures," *Sensors* **22**, 890 (2022).

168. K. J. Kataja et al., "Diffractive optical element in free-space data transmission systems," *Proc. SPIE* **3951**, 94–101 (2000).

169. P. Blattner et al., "Diffractive optics for compact space communication terminals," *J. Mod. Opt.* **43**, 1473–1484 (1996).

170. S.-Y. Yu et al., "Design of a combined functional phase-only diffractive element in intersatellite optical communications," *Proc. SPIE* **6021**, 60213W (2005).

171. J. Jia, C. Zhou, and L. Liu, "Superresolution technology for reduction of the far-field diffraction spot size in the laser free-space communication system," *Opt. Commun.* **228**, 271–278 (2003).

172. J. Wang and C. Xue, "Athermalization and thermal characteristics of multilayer diffractive optical elements," *Appl. Opt.* **54**, 9665–9670 (2015).

173. M. Piao et al., "Optimization method of multilayer diffractive optical elements with consideration of ambient temperature," *Appl. Opt.* **57**, 8861–8869 (2018).

174. A. Arbabi and A. Faraon, "Advances in optical metalenses," *Nat. Photonics* **17**, 16–25 (2022).

175. M. S. Islam et al., "Metalens wide-angle receiver for free space optical communications," *Proc. SPIE* **11814**, 1181409 (2021).

176. H. Tan et al., "A free-space orbital angular momentum multiplexing communication system based on a metasurface," *Laser Photonics Rev.* **13**(6), 1800278 (2019).

177. T. Dinter et al., "Metasurface measuring twisted light in turbulence," *ACS Photonics* **9**, 3043–3051 (2022).
178. F. Cheng et al., "Mechanically tunable focusing metamirror in the visible," *Opt. Express* **27**, 15194–15204 (2019).
179. Z. Guanxing et al., "Reconfigurable metasurfaces with mechanical actuations: towards flexible and tunable photonic devices," *J. Opt.* **23**, 013001 (2020).
180. T. Lewi, N. A. Butakov, and J. A. Schuller, "Thermal tuning capabilities of semiconductor metasurface resonators," *Nanophotonics* **8**, 331–338 (2019).
181. J. Young, "Advanced concepts for small satellite thermal control," in *Small Satell. Conf.* (2021).
182. R. C. Consolo and S. K. Boetcher, "Advances in spacecraft thermal control," *Adv. Heat Transf.* **56**, 1–50 (2023).
183. I. Garmendia et al., "Design and fabrication of a phase change material heat storage device for the thermal control of electronics components of space applications," *Aerospace* **9**, 126 (2022).
184. P. Kuruba, V. B. Rathnakar, and N. D. Dushyantha, "The future of thermal stability in small satellites using aerogel and graphene," in *AIP Conf. Proc.*, Vol. 2297 (2020).
185. M. Delkowski et al., "Multifunctional nanostructures with controllable band gap giving highly stable infrared emissivity for smart thermal management," *ACS Nano* **17**, 1335–1343 (2023).
186. L. Anderson et al., "CubeSat active thermal control in support of advanced payloads: the active thermal architecture project," *Proc. SPIE* **11832**, 1183203 (2021).

Mario Badás is a PhD candidate at Delft University of Technology. He received his BSc degrees in physics and engineering. He received his MSc degree in mechanical engineering in 2019 and his MSc degree in aerospace dynamics from the University of the Basque Country and Cranfield University, respectively. His current research interests include free-space optical and quantum communications, opto-thermo-mechanical phenomena, and multiphysics simulation.

Pierre Piron is an assistant professor at the Faculty of Aerospace Engineering of Delft University of Technology. He holds his PhD in optics focused on polarization from the University of Liege, Belgium. His research interests are the development of compact polarization components and measurement methods for spaceborne instruments.

Jasper Bouwmeester is an assistant professor at Delft University of Technology. He holds his MSc and PhD degrees in space systems engineering from Delft University of Technology and has more than 15 years of experience in end-to-end development of small satellites. His research interests comprise the system architecture of satellites, thermo-mechanical systems for innovative space instrumentation, and attitude sensors and actuators.

Jérôme Loicq is an associate professor at Delft University of Technology. He did his PhD in nonlinear optics and high-power lasers in cooperation at the Université Libre de Bruxelles, the University of Liège, and the Université Laval. Between 2004 and 2021, he worked as a researcher at the Space Center of Liège and a professor of space instrumentation at the University of Liège (since 2017). His research is mainly focused on spaceborne optical instruments.

Hans Kuiper is an assistant professor at Delft University of Technology. Previously, he held technical positions in the Dutch high-tech industry for more than 30 years. He holds his MSc degree in applied physics from Eindhoven University of Technology and his PhD in space systems engineering from Delft University of Technology. His research interest is in the systems engineering of spaceborne optical instruments.

Eberhard Gill is the chair of space systems engineering at the Faculty of Aerospace Engineering of Delft University of Technology and the head of the Department of Space Engineering. His research interests comprise the guidance, navigation, and control of distributed and miniaturized space systems and their engineering. He holds his PhD in theoretical astrophysics from the University of Tübingen, Germany.